

A Comparative Analysis of Contextual Representation Flow in State-Space and Transformer Architectures

Nhat M. Hoang¹, Do Xuan Long², Cong-Duy Nguyen¹, Min-Yen Kan², Luu Anh Tuan¹

¹Nanyang Technological University, Singapore,

²National University of Singapore

{hoangmin003, nguyentr003}@e.ntu.edu.sg,

xuanlong.do@u.nus.edu, kanmy@comp.nus.edu.sg, anhtuan.luu@ntu.edu.sg

Abstract

State Space Models (SSMs) have recently emerged as efficient alternatives to Transformer-Based Models (TBMs) for long-sequence processing with linear scaling, yet how contextual information flows across layers in these architectures remains understudied. We present the first unified, token- and layer-wise analysis of representation propagation in SSMs and TBMs. Using centered kernel alignment, variance-based metrics, and probing, we characterize how representations evolve within and across layers. We find a key divergence: TBMs rapidly homogenize token representations, with diversity reemerging only in later layers, while SSMs preserve token uniqueness early but converge to homogenization deeper. Theoretical analysis and parameter randomization further reveal that oversmoothing in TBMs stems from architectural design, whereas in SSMs, it arises mainly from training dynamics. These insights clarify the inductive biases of both architectures and inform future model and training designs for long-context reasoning.

1 Introduction

Long-context processing remains a critical challenge in natural language processing, with applications spanning document analysis, retrieval systems, and multi-turn dialogue (Beltagy et al., 2020; Goldman et al., 2024; Liu et al., 2025). While Transformer-Based Models (TBMs) (Vaswani et al., 2017) perform well, their quadratic complexity poses problems for scalability in long contexts (Gu and Dao, 2024). State Space Models (SSMs; i.e., Mamba) have emerged as promising linear-complexity alternatives, yet recent work has highlighted limitations in their long-context modeling (Jelassi et al., 2024; Chen et al., 2024).

Recent work has begun to probe the internal dynamics of these architectures (Fan et al., 2024; Skean et al., 2024; Ali et al., 2025; Skean et al.,

2025; Klabunde et al., 2025a; Skean et al., 2025; Men et al., 2025). For example, Skean et al. (2025) showed that intermediate layers often outperform final layers for task-relevant information in both TBMs and SSMs, challenging the conventional focus on final-layer outputs. Similarly, Wang et al. (2025) identified oversmoothing and recency bias in SSMs, where token representations converge as models favor local over distant context. However, it remains unclear how TBMs and SSMs fundamentally differ in propagating and transforming contextual representations across layers, particularly when token- and layer-wise perspectives are considered together. Prior studies have examined some aspects in isolation, but a unified characterization is lacking.

To bridge this gap, we present the first comprehensive empirical and theoretical pairwise comparison of representation flow in TBMs and SSMs. Our analysis spans local (token-wise; §3.2), global (layer-wise; §3.3), functional (probing; §3.4), and theoretical (§4) perspectives, with aligned setups and evaluation tasks enabling direct, side-by-side comparison. This reveals the architectural fingerprints that drive success or failure on long-context tasks and offers actionable guidance for future model and training design. Taken together, these findings lay the groundwork for hybrid architectures and model-specific optimizations, paving the way for more robust and efficient long-range reasoning. Our main contributions are:

- Unified layer-wise representation propagation.** We characterize token- and layer-wise dynamics, revealing opposing trends of diversity and homogenization in TBMs and SSMs.
- Architectural bias.** We show that oversmoothing in TBMs stems from architectural design, whereas in SSMs it arises primarily from training dynamics.

3. **Intermediate-layer effectiveness.** We find that intermediate layers from both architectures outperform final layers across tasks, model scales, and context lengths.
4. **Theoretical analysis.** Under practical assumptions, we provide a theoretical explanation for why SSMs empirically exhibit more stable representation propagation than TBMs.

2 Related Work

While TBMs (Vaswani et al., 2017) remain the dominant NLP architecture, their quadratic attention complexity limits scalability to long contexts.

SSMs offer a linear-complexity alternative, achieving efficiency gains in long-sequence tasks through compact state representations (Gu et al., 2022). However, recent studies reveal distinct architectural biases: SSMs often emphasize recency and local information, whereas TBMs maintain a broader contextual focus (Jelassi et al., 2024; Chen et al., 2024; Wang et al., 2025). These contrasting inductive biases motivate systematic analysis of how representations propagate within each family.

Recent work showed that intermediate layers often outperform final layers in both TBMs and SSMs, challenging the conventional reliance on final representations (Gao et al., 2024; Skean et al., 2025). Another study emphasized oversmoothing and recency bias in SSMs, where token representations gradually homogenize across layers (Wang et al., 2025). These findings suggest that models may fail to fully leverage all their layers, raising a question about how representations propagate across layers.

Layer-wise analyses commonly use Centered Kernel Alignment (CKA) (Kornblith et al., 2019) to measure representational similarity in TBMs (Conneau et al., 2020), while cosine similarity and variance-based metrics track feature evolution across layers. Probing further reveals where task-relevant information resides (Vulić et al., 2020; Gao et al., 2024). For example, probing on SSMs (Paulo et al., 2024) revealed that simple probes can recover correct knowledge even when fine-tuned outputs are incorrect, underscoring the richness of SSMs’ internal representations.

3 Empirical Analysis

We conduct a mechanistic analysis to study: (i) **token-wise analysis** (§3.2), which measures token-wise directional flow and token-set cohesiveness

across layers (cosine-based diagnostics); (ii) **layer-wise analysis** (§3.3), which cross-checks these local trends using global layer-geometry measures (CKA and layer-variation statistics); and (iii) **probing analysis** (§3.4), which evaluates where task-relevant information is most linearly accessible. The first two analyses provide insights into how models transform information, while probing analysis focuses on downstream performance.

3.1 Setup

Models. We evaluated models pre-trained on the Pile dataset (Gao et al., 2020) for a fair comparison, covering both TBM and SSM families. We include two TBMs, GPT-Neo-2.7B (Black et al., 2021) and Pythia-2.7B (Biderman et al., 2023); alongside three SSMs: Mamba2-2.7B (Dao and Gu, 2024), Mamba-2.8B, and a smaller Mamba2-130M. This selection enables both cross-architecture comparison and scaling effects within SSMs.

Tasks. We follow Liu et al. (2024) to adopt two benchmarks emphasizing long-range reasoning where models must process and retrieve information from extended contexts: (i) *Multi-Document Question Answering* (MDQA), where the input contains multiple documents and a question, requiring the model to identify the relevant document and answer; and (ii) *Key-Value Pair Retrieval* (KVPR), where the input contains multiple KV pairs represented as 128-bit random universally unique identifiers. The number of documents or KV pairs yields total context length $n \in \{300, 1K, 2K, 4K\}$. While absolute performance varies across tasks, we report averaged results across tasks as consistent representational trends are observed.

Probing Classifiers. For each input (instruction, documents/KV pairs, question), we extract its final token representation, $h_T^{(l)} \in \mathbb{R}^d$, from each Layer l where d is the hidden size, following prior work (Gao et al., 2024). In SSMs, the final token summarizes the entire context due to sequential state propagation. For each layer, we train a linear probe $f^l : \mathbb{R}^d \rightarrow \mathbb{R}^C$ to minimize the cross-entropy loss:

$$\mathcal{L}^l := -\frac{1}{M} \sum_{i=1}^M \sum_{c=1}^C y_{i,c} \log(\hat{y}_{i,c}^l) \quad (1)$$

where C is the number of classes (e.g., number of KV pairs in KVPR), M is the number of train

samples, $y_{i,c}$ is the true label and $\hat{y}_{i,c}^l$ is the softmax prediction of data sample i .

Implementation Details. We use pre-trained checkpoints of TBMs and SSMs from the Hugging Face (Wolf et al., 2020). All probes are trained from frozen representations for 150 epochs using Adam optimizer (Kingma and Ba, 2015) with a learning rate of 0.05 on the full $20K$ -sample training set (no batching), with evaluation on a held-out validation split. Reported results are mean accuracies over five random seeds across both tasks, under consistent hyperparameters and evaluation protocols on NVIDIA L40S GPUs.

3.2 Token-Wise Analysis

Our token-wise analysis aims to understand: (i) how smoothly representations evolve across layers; (ii) whether tokens maintain their distinctiveness or become homogenized within layers; and (iii) whether these behaviors arise from architectural biases or training dynamics.

Setup. To track token representations’ dynamics in TBMs and SSMs, we employ three complementary cosine-similarity-based analyses. Cosine similarity is used here because it is widely adopted in prior representational studies, and can provide valuable insights into directional flow of representations in the model’s native parameterization (Ethayarajh, 2019; Lauscher et al., 2020), and it is rotational and scale invariance (Smith et al., 2023).

First, we compute *adjacent-layer cos. similarity* to measure the layer-wise directional alignment of each token across consecutive layers. For a token representation $h_t^{(l)} \in \mathbb{R}^d$ at layer l and position t :

$$\text{Sim}(h_t^{(l)}, h_t^{(l+1)}) = \frac{h_t^{(l)} \cdot h_t^{(l+1)}}{\|h_t^{(l)}\| \|h_t^{(l+1)}\|}$$

which indicates how strongly the representation direction is *preserved* (high values) versus *changed* (low/negative values), from Layer l to $l+1$.

Second, we compute *inter-token cosine similarity* within each layer to assess token-set cohesiveness, a proxy for oversmoothing (Ali et al., 2024). Given $h^{(l)} \in \mathbb{R}^{n \times d}$, we compute:

$$\text{InterSim}^{(l)} := \frac{2}{n(n-1)} \sum_{i=1}^n \sum_{j=i+1}^n \frac{h_i^{(l)} \cdot h_j^{(l)}}{\|h_i^{(l)}\| \|h_j^{(l)}\|} \quad (2)$$

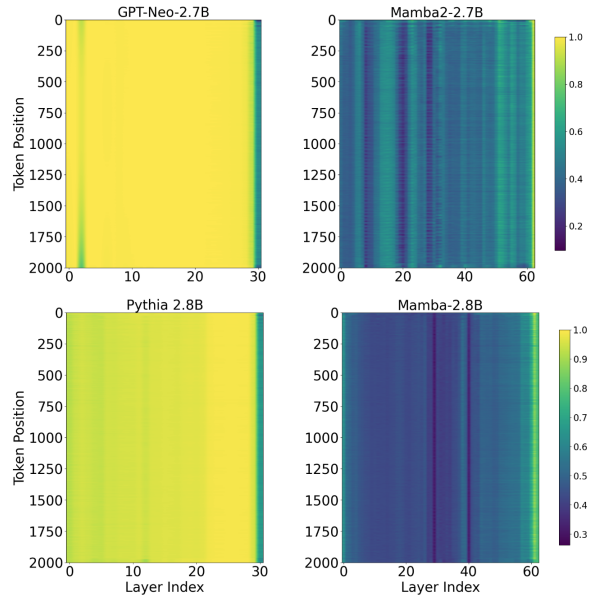


Figure 1: **Distinct representation dynamics of TBMs (left) and SSMs (right).** TBMs maintain consistently high layer-wise similarity until a sharp shift near the final layers, indicating stable token evolution followed by more abstract refinement. In contrast, SSMs reveal greater variability and exploratory changes in early layers, with gradual convergence later.

which reflects the average pairwise similarity among tokens, excluding self-similarity. Higher values indicate increased alignment among token representations and reduced token distinctiveness, indicative of oversmoothing.

Finally, to **disentangle training artifacts from architectural priors**, we analyze both pretrained and randomly initialized models. For random initialization, we explore multiple schemes including Gaussian, Xavier (Glorot and Bengio, 2010), and He Kaiming (He et al., 2015)s. This allows us to isolate oversmoothing tendencies inherent to the architecture itself.

All analyses are performed on MDQA and KVPR with context length $n = 2K$ tokens, matching the effective window size of GPT-Neo-2.7B and Pythia-2.8B.

3.2.1 Token Evolution Across Layers.

Figure 1 reveals clear differences in how token representations evolve through layers within the two architectures, though the overall trend remains consistent across tokens within each model (i.e., all rows follow a similar pattern). For GPT-Neo-2.7B, similarity starts at nearly 100%, dips slightly to 90% by Layer 3, quickly recovers to 100%, and holds steady until a sharp decline to 70%

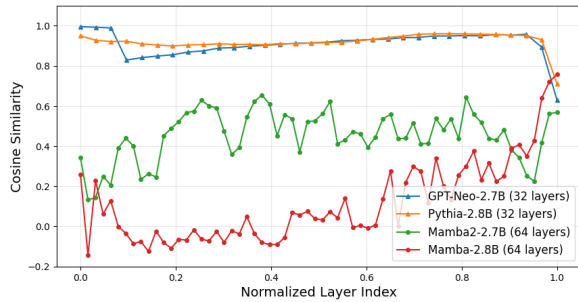


Figure 2: **TBMs oversmooth early then recover late while SSMS preserve token diversity longer.** TBMs rapidly increase token similarity early and maintain high homogenization until a late drop. Conversely, SSMS sustain greater token diversity through most layers, with only a late-stage increase in similarity.

at Layer 32. Similarly, Pythia-2.8B begins at $\sim 90\%$, gradually increases to $\sim 100\%$ by Layer 23, but also drops from Layer 29 to 70% by the final layer, mirroring GPT-Neo-2.7B’s late shift. In contrast, Mamba2-2.7B fluctuates between 20% and 40% until Layer 51, reflecting diverse directional changes, before rising steadily to 80% by the last Layer 64. Meanwhile, Mamba-2.8B displays a unique elbow pattern: starting at 30%, it drops to 0% or even negative values at Layers 30 and 41, then gradually rises to $\sim 60\%$ by the final layer. This suggests that while TBMs prioritize stability and preservation, SSMS promote continual token evolution and refinement. Such dynamism may be critical for maintaining expressivity in deep models, particularly for long-context tasks.

F 3.2.1. TBMs exhibit stable token evolution until a sharp final-layer shift, contrasting with SSMS’ varied directions that are converged in later layers.

3.2.2 Token Uniqueness Within Layers

Figure 2 highlights differences in token distinctiveness inside layers. TBMs, GPT-Neo-2.7B (blue line) and Pythia-2.8B (orange line), maintain high inter-token similarity across most layers (around 90%), indicative of oversmoothing where token representations become increasingly alike. Both models experience a significant reduction to roughly 60% near the final layer (normalized layer index = 1.0), reaching substantially lower similarity, which indicates a late-stage resurgence of token diversity. In contrast, SSMS such as Mamba2-2.7B (green line) and Mamba-2.8B (red line) stay much lower through most of the net-

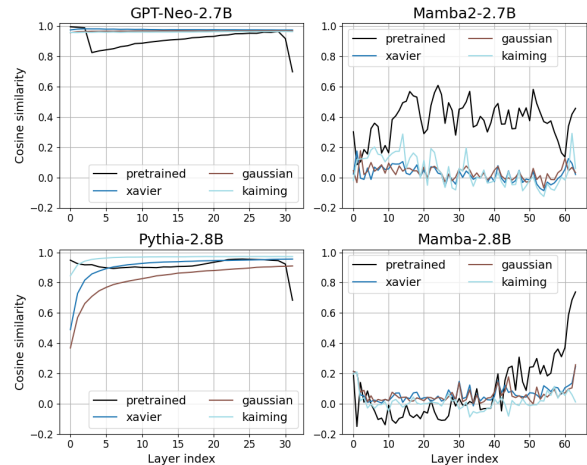


Figure 3: **Architectural bias on the oversmoothing problem of TBMs (left) and SSMS (right).** TBMs show high similarity regardless of initializations, following the pre-trained model. In contrast, SSMS exhibits near-zero similarity at random initializations.

work (around 50% and 5% respectively), preserving token uniqueness longer. Notably, Mamba-2.8B (red) shows an increase in similarity beginning around Layer 40, reaching 70% by the final layer, while Mamba2-2.7B (green) sustains lower similarity throughout. These trends underscore SSMS’ ability to preserve token individuality longer than TBMs, which homogenize early.

F 3.2.2. TBMs collapse token distinctions early and recover diversity late, while SSMS maintain the uniqueness longer. xc x

3.2.3 Architectural Bias On The Oversmoothing Problem

Figure 3 isolates architectural bias by comparing pre-trained (black) models with randomly initialized (colored) counterparts. In the left panel, TBMs exhibit consistently high token similarity for both the pre-trained curve and all random initializations (Xavier/Gaussian/Kaiming): similarity rises rapidly to $\sim 80-100\%$ within the first few layers and remains saturated after, indicating that oversmoothing is fundamentally driven by the TBM architecture. In contrast, SSMS behaves differently: the random-initialization curves stay near zero throughout most layers, whereas the pre-trained curve is substantially higher and increases again near the final layer, implying that oversmoothing in SSMS is primarily learned through training rather than being purely architectural.



F 3.2.3. Oversmoothing in TBMs is an intrinsic architectural, while in SSMs it is primarily a consequence of training or optimization process.

3.3 Layer-Wise Analysis

This analysis aims to answer two key questions: (i) how similar are the sets of token representations between any two layers (global structure), and (ii) how much these representations change on average as we move through the layers of the models. Understanding these clarifies whether long-range dependencies are preserved or degraded as representations propagate through the network.

Setup. To compare layer-wise representations, we adopt the CKA metric (Kornblith et al., 2019) to measure similarity between layer representations. Specifically, we define two layer variance measures: **Layer-local** V_{loc} and **Layer-global Variance** V_{glob} :

$$V_{\text{loc}} := \frac{1}{n \cdot d} \sum_{t=1}^{n \cdot d} \left(\frac{1}{L-2} \sum_{l=0}^{L-2} \left| h^{(t+1)} - \frac{h^{(l)} + h^{(l+2)}}{2} \right| \right) \quad (3)$$

$$V_{\text{glob}} := \frac{1}{n \cdot d} \sum_{t=1}^{n \cdot d} \sqrt{\frac{1}{L} \sum_{l=1}^L (h^{(l)} - \bar{h})^2} \quad (4)$$

where \bar{h} represents the mean layer representation across all L layers.

V_{loc} captures short-range changes between adjacent layers (a measure of local ‘‘curvature’’), whereas V_{glob} summarizes the overall variation across all layers relative to their mean representation. Lower values indicate smaller representation flow in the model’s parameterization; these metrics are interpreted comparatively (TBM vs SSM) and together with CKA, rather than as intrinsic manifold distances. The analyses are conducted under the same task setup and context length as in the token-wise experiments to ensure comparability.

3.3.1 Layer-wise Representation Dynamics

Figure 4 shows that GPT-Neo-2.7B maintains near-perfect CKA similarity ($\sim 100\%$) in early layers, with even the first layer retaining 90% similarity with Layer 20. Consistent with observations in Section 3.2, a feature shift occurs at Layer 29, where the similarity score drops to 80% by the final layer. This suggests the manifold formed by token representations is stable and smoothly transforms before undergoing reconfiguration in late layers. In

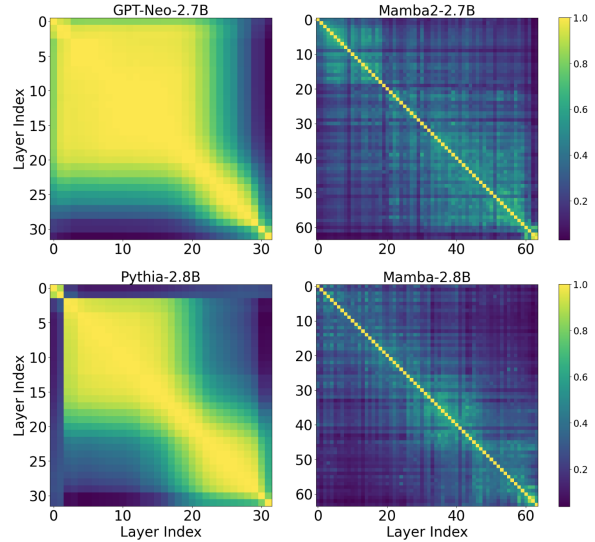


Figure 4: Layer-wise CKA similarity for every layer pair, averaged over the MDQA and KVPR tasks with $n = 2K$ tokens. TBMs (left) exhibit stable alignment across initial layers (except for Layer 1–2 of Pythia-2.8B), followed by a representation shift towards the final layers, with lower similarity between the early and final layers. In contrast, SSMs (right) show significant fluctuation in the lower layers, followed by a more consistent alignment in deeper layers, indicating a gradual stabilization of feature representations.

Model	$n = 300$	$n = 1K$	$n = 2K$	$n = 4K$
	Prob Acc. \uparrow	Prob Acc. \uparrow	Prob Acc. \uparrow	Prob Acc. \uparrow
GPT-Neo-2.7B	88.7 ($\downarrow 10.9$)	70.7 ($\downarrow 18.7$)	53.1 ($\downarrow 25.3$)	-
Pythia-2.8B	95.9 (13.8)	72.3 ($\downarrow 14.0$)	60.9 ($\downarrow 15.4$)	-
Mamba2-130M	72.5 ($\downarrow 17.1$)	42.3 ($\downarrow 13.8$)	28.6 ($\downarrow 18.0$)	20.6 ($\downarrow 7.6$)
Mamba-2.8B	93.0 ($\downarrow 6.4$)	62.5 ($\downarrow 11.7$)	41.7 ($\downarrow 14.0$)	36.7 ($\downarrow 12.2$)
Mamba2-2.7B	86.0 ($\downarrow 13.5$)	57.2 ($\downarrow 17.6$)	38.2 ($\downarrow 20.6$)	29.7 ($\downarrow 13.3$)

Table 1: Probing accuracy (%) using the **last layer’s representation**. We run all evaluations 5 times and report the average. ($\downarrow x$) is the accuracy difference between the probe trained on the last layer and on the **peak layer**. The best results are **bolded**.

Model	$n = 300$		$n = 1K$		$n = 2K$		$n = 4K$	
	$V_{\text{loc}} \downarrow$	$V_{\text{glob}} \downarrow$						
GPT-Neo-2.7B	0.938	3.635	0.980	3.833	0.979	3.821	-	-
Pythia-2.8B	0.265	1.059	0.277	1.122	0.280	1.147	-	-
Mamba2-130M	3.572	5.395	3.704	5.665	3.752	5.735	3.846	5.890
Mamba-2.8B	0.173	0.315	0.189	0.354	0.193	0.363	0.190	0.354
Mamba2-2.7B	1.945	3.238	1.939	3.288	1.932	3.275	1.897	3.193

Table 2: Layer-local Variance V_{loc} and Layer-global Variance V_{glob} , reported across context lengths. Lower is better (less variation), the best results are **bolded**.

contrast, Pythia-2.8B starts at 90% similarity but drops sharply to 30% by the second layer. However, its propagation pattern in the remaining layers (3–32) closely resembles that of GPT-Neo-2.7B. In contrast, both Mamba2-2.7B and Mamba-2.8B exhibit fluctuating similarity scores between 20%

and 70% until Layer 51, after which they steadily increase, reaching 90% by the final Layer 64. This difference signals distinct architectural strategies in maintaining and reshaping feature spaces at a global level, revealing their contrasting approaches to integrating and refining context beyond individual token trajectories.

 **F 3.3.1.** TBMs maintain globally similar layer representations early while SSMs gradually refine global structure towards late-layer stabilization.

3.3.2 Comparative Analysis of V_{loc} and V_{glob}

Table 2 reveals that among SSMs, only Mamba-2.8B consistently achieves lower V_{loc} (~ 0.19) and V_{glob} (~ 0.34) values compared to the TBMs (Pythia-2.8B: $\sim 0.27 V_{loc}$ and $\sim 1.11 V_{glob}$; GPT-Neo-2.7B: $\sim 0.97 V_{loc}$ and $\sim 3.76 V_{glob}$), indicating a more gradual and stable evolution of its representations. This behavior may stem from Mamba-2.8B’s smaller state size, which may constrain its capacity to model diverse token features, resulting in smoother transitions across layers. In contrast, Mamba2-2.7B, with an $8\times$ larger state size, shows higher V_{loc} and V_{glob} values than Pythia-2.8B, suggesting that increased state dimensions amplify representation variability and reduce stability, potentially leading to more abrupt changes. Among TBMs, Pythia-2.8B exhibits V_{loc} and V_{glob} values roughly three times lower than GPT-Neo-2.7B, indicating that Pythia-2.8B’s architectural refinements foster smoother and more stable feature propagation. These findings underscore how design choices, even within the same model family, significantly influence representation dynamics.

 **F 3.3.2.** The variance of representation evolution depend on model-specific factors like scale and parameterization rather than architecture type.

3.4 Probing Analysis

This analysis measures how well task-relevant information can be utilized at each layer, which complements the analyses in §3.2 and §3.3.

3.4.1 Intermediate Layers Outperform The Final Layer

Table 1 and Figure ?? show that GPT-Neo-2.7B and Pythia-2.8B achieve peak accuracy around Layer 10 (out of 32) before dropping by up to 26%

in the final layer. Mamba2-2.7B peaks between Layers 4 and 14 (out of 64) and declines by up to 13.9%. In contrast, Mamba-2.8B reaches its peak later, around Layer 28 or beyond (out of 64), with a more gradual drop of at most 10.5% by the final layer.

 **F 3.4.1.** Task-relevant representations peak in intermediate layers for both architectures, with SSMs having a smaller gap to the last layer than TBMs.

3.4.2 Effect of Context Length

Table 2 shows that while V_{loc} and V_{glob} metrics remain stable across context lengths ranging from 300 to 4K tokens, probing accuracy steadily declines with increasing input length. This suggests that although internal representations evolve predictably, model capacity constraints limit the ability to retain task-relevant information in longer sequences. This trend holds consistently across models and tasks, illustrating a key trade-off between representational stability and capacity to capture extended context.

 **F 3.4.2.** Despite stable representation evolution across varied context lengths, probing accuracy decreases as context length increases, indicating capacity limitations rather than representation instability.

3.4.3 Effect of Model Size

Comparing the smaller (Mamba2-130M) and larger (Mamba2-2.7B) SSM variants reveals that the larger model significantly improves final-layer probing accuracy, particularly for longer contexts (by 2.3% in the 4K MDQA task and 15.9% in the 4K KVPR task). While its intermediate layers capture richer representations, they also exhibit a larger accuracy drop toward the final layer (increasing from 6.7% to 13.3% in MDQA and from 24.0% in KVPR), indicating a more aggressive transformation that may discard fine-grained details. Nonetheless, the overall improvement in task performance suggests that deeper processing benefits outweigh this loss.

 **F 3.4.3.** While larger model size generally improves task performance, final-layer representations tend to become more abstract, which might reduce accessibility to certain fine-grained intermediate features.

4 Theoretical Analysis

We provide a theoretical analysis to explain our empirical patterns observed in §3. We start on the expected value of the layer-global variance metric $\mathbb{E}[V_{\text{glob}}^2]$ (Eq. 4) over a single layer ($L = 1$) to compare the variance of TBM and SSM, then generalize the result to L -layer model in Appendix A.3. For TBMs, we analyze a simplified single-head self-attention + FFN block (Eq. 5); For SSMs, we use Mamba’s formulas as a representative case study.

4.1 Backgrounds and Setups

Backgrounds. Given an input sequence $x = [x_1, x_2, \dots, x_n]$ of length n , where x_i are tokens coming from a finite vocabulary \mathcal{V} , the Transformer (Vaswani et al., 2017) processes it as follows. Initially, each token x_i is mapped to a d -dimensional vector $v_i = \text{Embed}(x_i) \in \mathbb{R}^d$ using an embedding layer. To encode positional information, a positional embedding $p_i \in \mathbb{R}^d$ is added to the token representation. The resulting embedded sequence is expressed as a matrix $h^{(0)} = [h_1^{(0)}, \dots, h_n^{(0)}]^T \in \mathbb{R}^{n \times d}$ where $h_i^{(0)} = v_i + p_i$. Subsequently, the sequence passes through L_t transformer blocks, each of which applies the following transformation:

$$h^{(l)} := h^{(l-1)} + \text{Attn}(h^{(l-1)}) + \text{FFN}(h^{(l-1)} + \text{Attn}(h^{(l-1)})) \quad (5)$$

where Attn, FFN stand for single-head self-attention, and feed-forward layers. Note that we use the single-head self-attention instead of multi-head attention, and we skip the layer normalization layers for simplicity following Feng et al. (2023). We also skip the layer normalization in the SSM formulations in Equation 6 below.

With the same input matrix $h^{(0)}$, Mamba also passes it through L_m layers where L_m typically larger than L_t :

$$h^{(l)} := h^{(l-1)} + g^{(l)} \left(\text{S6}(f^{(l)}, h^{(l-1)}) \circ z^{(l)} \right) \quad (6)$$

here S6 is the selective SSM transformation, $g^{(l)}$ is a linear transformation, and $z^{(l)} = \text{SiLU}(\text{Linear}(h^{(l-1)}))$.

Setups. We consider the case where $L = 1$ following Feng et al. (2023); Kajitsuka and Sato

(2024). The variance-based metric St^2 (Eq. 4) is then defined as:

$$V_{\text{glob}}^2 \propto \|h^{(1)} - h^{(0)}\|^2, \quad (7)$$

where $h^{(l)}$ is the representation at Layer l . To enable our analysis, we make the following assumptions:

Assumption 1 (Random initial representations). *The initial representation $h^{(0)} \in \mathbb{R}^{n \times d}$ is a Gaussian matrix with $\mathbb{E}[h^{(0)}] = 0$ and covariance $\text{Cov}(h^{(0)}) = \sigma^2 I$, where each $h_i^{(0)} \sim N(0, \sigma^2 I)$.*

Assumption 2 (Independence). *The token representations $h_j^{(0)}$ and $h_t^{(0)}$ are independent for $j \neq t$ (i.e., $\mathbb{E}[h_j^{(0)}(h_t^{(0)})^T] = 0$).*

Assumption 3 (Deterministic parameters). *Model parameters (e.g., weight matrices) are deterministic, with randomness stemming solely from $h^{(0)}$.*

Assumption 4 (Non-linearity approximations). *Non-linear functions (e.g., GELU in TBMs, SiLU in Mamba) are approximated via Taylor expansion as $\text{GELU}(x) \approx \frac{1}{2}x$ and $\text{SiLU}(x) \approx \frac{1}{2}x$ to simplify the computations.*

Note that Assumption 4 is reasonable because the initial representations x of both models are close to the zero vector,

4.2 Theoretical Results

Let $F : \mathbb{R}^{n \times d} \rightarrow \mathbb{R}^{n \times d}$ denote a function that transforms an input matrix $h^{(0)} \in \mathbb{R}^{n \times d}$ into an output matrix $h^{(1)} = F(h^{(0)})$, where n represents the number of rows (e.g., sequence length) and d represents the number of columns (e.g., feature dimension). For a TBM, let $V_{\text{glob, Trans}}^2$ denote the variance metric, with $\Sigma_{F, \text{Trans}}$ as the covariance matrix and $\mu_{F, \text{Trans}}$ as the mean vector of the output of the Transformer function F . For a Mamba model, let $V_{\text{glob, Mamba}}^2$ denote the squared variance metric, with $\Sigma_{F, \text{Mamba}}$ as the covariance matrix and $\mu_{F, \text{Mamba}}$ as the mean vector of the output of the Mamba function F . We aim to prove that $\mathbb{E}[V_{\text{glob, Trans}}^2] > \mathbb{E}[V_{\text{glob, Mamba}}^2]$.

Proposition 1. *Consider F (e.g., Mamba or Transformer) with input matrix $h^{(0)}$. Then, the expected variance satisfies*

$$\mathbb{E}[V_{\text{glob}}^2] \propto \mathbb{E}[\|F(h^{(0)})\|_F^2] = \text{Tr}(\Sigma_F) + \|\mu_F\|_F^2, \quad (8)$$

where $\mu_F = \mathbb{E}[F(h^{(0)})]$ is the mean representation, $\Sigma_F = \text{Cov}[F(h^{(0)})]$ is the covariance, and $\|\cdot\|_F$ denotes the Frobenius norm.

Proposition 2. *The attention function is odd, i.e.,*

$$\text{Attn}(-x) = -\text{Attn}(x). \quad (9)$$

Proposition 3. *For zero-mean inputs $h^{(0)}$, the expected attention output vanishes:*

$$\mathbb{E}[\text{Attn}(h^{(0)})] = 0. \quad (10)$$

Theorem 1. *Let $\tilde{h}^{(0)} = h^{(0)} + \text{Attn}(h^{(0)})$ and consider the feed-forward layer*

$$\text{FFN}(\tilde{h}^{(0)}) = W_2 \text{GELU}(W_1 \tilde{h}^{(0)} + b_1) + b_2,$$

where W_1, W_2, b_1, b_2 are independent. Then, the expected output of the feed-forward block is approximately

$$\mu_{F,Trans} \approx \frac{1}{2} W_2 b_1 + b_2. \quad (11)$$

Theorem 2. *Let $F_{Trans} = \text{Attn}(h^{(0)}) + \text{FFN}(\tilde{h}^{(0)})$ and given that $\text{Attn}(h^{(0)})$ is odd and $h^{(0)}$ is symmetrically distributed around zero, the bias terms do not affect the covariance. We have:*

$$\begin{aligned} \text{Tr}(\Sigma_{F,Trans}) &= \sigma^2 \text{Tr}(T_1 T_1^\top) + n \sigma^2 \text{Tr}(T_2 T_2^\top) \\ &\quad + 2\sigma^2 \text{Tr}(T_1 W_V T_2^\top) \end{aligned} \quad (12)$$

where $T_1 = I + \frac{1}{2} W_2 W_1$, $T_2 = \frac{1}{2} W_2 W_1$

Theorem 3. *Let $W_{h'_j} = W_{c_j} W_h$, where W_{c_j} is a causal convolution of kernel size j and W_h is a linear projection. Then, the expected output of the Mamba block satisfies*

$$\mu_{F,Mamba} = \frac{\sigma^2}{4n} \sum_{t=1}^n \text{diag}(C_t \bar{B}_t W_{h'_0} W_z^\top), \quad (13)$$

where $C_t, \bar{B}_t, W_{h'}$, and W_z are Mamba parameters computed via the SiLU approximation and SSM recursion.

Theorem 4. *For $1 \leq t, j \leq n$, let $M_{t,j} = C_t \left(\prod_{k=j+1}^t \bar{A}_k \right) \bar{B}_j W_{h'}$. Then, the trace of the covariance of the Mamba block is*

$$\begin{aligned} \text{Tr}(\Sigma_{F,Mamba}) &= \frac{\sigma^4}{4} \left\{ \text{Tr}[(W_z W_z^\top) \circ S_t] \right. \\ &\quad \left. + \text{Tr}[(M_{t,t} W_z^\top) \circ (W_z M_{t,t}^\top)] \right\} \end{aligned} \quad (14)$$

where $S_t = \sum_{j=1}^{t-1} M_{t,j} M_{t,j}^\top$ and \bar{A}_k is a Mamba parameter.

Theorem 5. *In addition to Assumptions 1–4, we impose an extra condition to bound the Mamba parameters. Specifically, we assume that Mamba is uniformly contractive: there exists $\rho \in (0, 1)$ such that $\|\bar{A}_t\|_2 \leq \rho$ for all t , and that the operator and Frobenius norms are bounded as $\|C_t\|_2 \leq c$, $\|\bar{B}_t\|_2 \leq b$, $\|W_{h'}\|_2 \leq h$, and $\|W_z\|_F \leq z$.*

Under these conditions, it holds that

$$\mathbb{E}[V_{glob, Trans}^2] > \mathbb{E}[V_{glob, Mamba}^2] \quad \forall n \geq 1. \quad (15)$$

Proofs for the above propositions and theorems are provided in §A.2. In summary, Theorem 5 provides a qualitative explanation for the representation flow and stabilization patterns observed in §3. It shows that, when layers are contractive, SSM blocks admit tighter variance bounds than TBM blocks. This explains the gradual stabilization of SSM representations (Findings 3.2.1, 3.3.1) and their stronger dependence on parameterization (Finding 3.3.2).

5 Conclusions

We present a unified token- and layer-wise comparison of representation flow in TBMs and SSMs, revealing opposing oversmoothing trajectories: TBMs homogenize early then recover, while SSMs preserve early token uniqueness but converge to homogenization deeper. This divergence explains why both architectures can perform well yet fail differently as context grows, shifting the focus from “which is better” to how each routes and re-encodes information across depth. Our analysis also yields practical diagnostics: intermediate layers often contain the most usable knowledge, and combining layerwise probes with V_{loc}/V_{glob} and inter-token similarity metrics can flag failures before deployment. These findings motivate targeted interventions (e.g., intermediate supervision, contrastive regularization, contractive constraints) and suggest a concrete hybrid design principle: place SSM blocks early to preserve token diversity, then apply attention blocks late to reintroduce global mixing. A natural next step is to implement and systematically evaluate such hybrids under controlled long-context benchmarks to validate these design choices. Finally, we provide a reproducible toolkit of similarity measures, variance-based analysis, and layer-wise evaluation to support future work on multimodal tasks, hybrid architectures, and long-context modeling.

Limitations

While our study sheds light on representation flow in SSMs and TBMs, we acknowledge several limitations. First, cosine similarity has several limitations: (i) it is sensitive to non-orthogonal reparameterizations that can alter angular alignment without changing functional behavior; (ii) adjacent-layer cosine in residual architectures is biased upward by skip connections, which introduce background similarity even when updates are large; and (iii) it captures only local directional changes and cannot fully characterize global manifold structure or information content. In this work, it is worth noting that we interpret cosine strictly as a directional flow diagnostic in the model’s native parameterization and require its trends to align with rotation/scale-invariant CKA and functional probing results (Steck et al., 2024; Kornblith et al., 2019). While orthogonal invariance holds mathematically, trained TBMs and SSMs lack orthogonal symmetries due to nonlinearities and normalization, so cosine remains empirically informative for layerwise comparisons (Klabunde et al., 2025b). Moreover, we apply the same metric consistently to both TBMs and SSMs and focus on differential patterns across architectures. Consequently, even if residual connections introduce an absolute similarity offset, our analysis depends on comparative dynamics rather than absolute similarity values.

In addition, our findings are limited to the specific tasks and models examined. While MDQA and KVPR capture key aspects of long-context reasoning, they might not exhaust the range of settings in which TBMs and SSMs are applied. Likewise, although we evaluate four representative Pile-trained models under controlled and comparable conditions, this scope might limit the generality of our conclusions. Extending our analysis to a broader set of tasks, architectures, training regimes, and data sources remains an important direction for future work to assess the robustness and universality of the observed representation dynamics.

Ethics Considerations

Our research does not involve human subjects, personal data collection, or direct societal applications that could cause harm. However, we acknowledge that our findings about representation flow and layer-wise performance could potentially be misused for adversarial purposes, though they primarily enable beneficial applications such as more

efficient model design. Our analysis uses models trained on the Pile dataset, which may contain societal biases that could be reflected in the representation patterns we observe, and future work should consider how architectural differences interact with bias mitigation strategies. While this research contributes to fundamental understanding that may inform more efficient language models with societal benefits, it also raises broader considerations about computational resource concentration and the responsible development of increasingly capable AI systems.

Significance of Our Findings

Our analysis uncovers a fundamental divergence in how SSMs and TBMs propagate information across layers, revealing an architecture-level trade-off that reframes long-context modeling. By showing that TBMs and SSMs follow opposite over-smoothing trajectories—TBMs exhibit early homogenization followed by late recovery, while SSMs preserve early uniqueness but suffer late homogenization—we explain why architectures that both perform well on language tasks nonetheless fail in systematically different ways as context grows. This insight transforms debates about "which family is better" into the more productive question of how each family routes and re-encodes information across layers.

Our findings provide concrete diagnostics for common failure modes. The empirical and theoretical link between layerwise representation flow and probing accuracy explains why final-layer readouts can be misleading and why intermediate layers often contain the most usable knowledge. This enables a reliable diagnostic pipeline: layerwise probes combined with $V_{\text{loc}}/V_{\text{glob}}$ and inter-token similarity metrics can detect whether a model will lose token-wise detail or over-compress context before deployment.

These insights point to immediate, practical interventions. Because representational collapse occurs at predictable layers, we can target fixes precisely: intermediate supervision, contrastive regularization to maintain token distinctiveness, contractive constraints for SSM dynamics, and hybrid architectures that route early processing through SSMs and global reconfiguration through attention. Our analysis also informs scaling strategies, showing that larger state dimensions can destabilize representations, providing principled guidance

for when and where to scale capacity.

Finally, our work establishes a new experimental toolkit. The $V_{\text{loc}}/V_{\text{glob}}$ similarity measures, comparative variance bounds, and layerwise analysis framework provide the community with reproducible metrics and theory-backed baselines for rigorous architecture comparison, opening avenues for provable regularizers, architecture-aware training, and benchmarks tailored to layerwise information retention.

Future Directions

Our findings open several promising directions. First, while our analysis focused on text-based sequence modeling, it would be valuable to extend the framework to multimodal domains such as video or speech, where long-context fidelity is equally critical. Second, integrating our similarity measures into the training loop may enable adaptive regularization schemes that detect and counteract oversmoothing in real time. Third, hybrid architectures that combine the local retention of SSMs with the global reconfiguration capacity of TBMs remain largely unexplored; systematic exploration of such designs could yield models with both efficiency and fidelity. Finally, future research could investigate scaling laws under these new diagnostics, asking how model size, layers, and state dimensionality interact with representation collapse across architectures. Together, these directions point toward a principled roadmap for developing the next generation of long-context models.

Acknowledgements

We thank members in NAIL (NTU) and WING (NUS) labs for their valuable feedback. Do Xuan Long is supported by the A*STAR Computing and Information Science Scholarship.

References

- Ameen Ali, Itamar Zimmerman, and Lior Wolf. 2024. The hidden attention of mamba models. *arXiv preprint arXiv:2403.01590*.
- Ameen Ali, Itamar Zimmerman, and Lior Wolf. 2025. The hidden attention of mamba models. In *Proceedings of the 63rd Annual Meeting of the Association for Computational Linguistics (Volume 1: Long Papers)*, pages 1516–1534.
- Iz Beltagy, Matthew E. Peters, and Arman Cohan. 2020. Longformer: The long-document transformer. *arXiv:2004.05150*.
- Stella Biderman, Hailey Schoelkopf, Quentin Gregory Anthony, Herbie Bradley, Kyle O’Brien, Eric Hallahan, Mohammad Aflah Khan, Shivanshu Purohit, Usven Sai Prashanth, Edward Raff, Aviya Skowron, Lintang Sutawika, and Oskar Van Der Wal. 2023. *Pythia: A suite for analyzing large language models across training and scaling*. In *Proceedings of the 40th International Conference on Machine Learning*, volume 202 of *Proceedings of Machine Learning Research*, pages 2397–2430. PMLR.
- Sid Black, Leo Gao, Phil Wang, Connor Leahy, and Stella Biderman. 2021. *GPT-Neo: Large Scale Autoregressive Language Modeling with Mesh-Tensorflow*.
- Yingfa Chen, Xinrong Zhang, Shengding Hu, Xu Han, Zhiyuan Liu, and Maosong Sun. 2024. *Stuffed mamba: State collapse and state capacity of rnn-based long-context modeling*. *arXiv preprint arXiv:2410.07145*.
- Alexis Conneau, Shijie Wu, Haoran Li, Luke Zettlemoyer, and Veselin Stoyanov. 2020. *Emerging cross-lingual structure in pretrained language models*. In *Proceedings of the 58th Annual Meeting of the Association for Computational Linguistics*, pages 6022–6034, Online. Association for Computational Linguistics.
- Tri Dao and Albert Gu. 2024. *Transformers are SSMs: Generalized models and efficient algorithms through structured state space duality*. In *Forty-first International Conference on Machine Learning*.
- Kawin Ethayarajh. 2019. *How contextual are contextualized word representations? Comparing the geometry of BERT, ELMo, and GPT-2 embeddings*. In *Proceedings of the 2019 Conference on Empirical Methods in Natural Language Processing and the 9th International Joint Conference on Natural Language Processing (EMNLP-IJCNLP)*, pages 55–65, Hong Kong, China. Association for Computational Linguistics.
- Siqi Fan, Xin Jiang, Xiang Li, Xuying Meng, Peng Han, Shuo Shang, Aixin Sun, Yequan Wang, and Zhongyuan Wang. 2024. *Not all layers of llms are necessary during inference*. *arXiv preprint arXiv:2403.02181*.
- Guhaog Feng, Bohang Zhang, Yuntian Gu, Haotian Ye, Di He, and Liwei Wang. 2023. *Towards revealing the mystery behind chain of thought: A theoretical perspective*. In *Thirty-seventh Conference on Neural Information Processing Systems*.
- Leo Gao, Stella Biderman, Sid Black, Laurence Golding, Travis Hoppe, Charles Foster, Jason Phang, Horace He, Anish Thite, Noa Nabeshima, et al. 2020. *The pile: An 800gb dataset of diverse text for language modeling*. *arXiv preprint arXiv:2101.00027*.
- Muhan Gao, TaiMing Lu, Kuai Yu, Adam Byerly, and Daniel Khashabi. 2024. *Insights into LLM long-context failures: When transformers know but don’t*

- tell. In *Findings of the Association for Computational Linguistics: EMNLP 2024*, pages 7611–7625, Miami, Florida, USA. Association for Computational Linguistics.
- Xavier Glorot and Yoshua Bengio. 2010. [Understanding the difficulty of training deep feedforward neural networks](#). In *Proceedings of the Thirteenth International Conference on Artificial Intelligence and Statistics*, volume 9 of *Proceedings of Machine Learning Research*, pages 249–256, Chia Laguna Resort, Sardinia, Italy. PMLR.
- Omer Goldman, Alon Jacovi, Aviv Slobodkin, Aviya Maimon, Ido Dagan, and Reut Tsarfaty. 2024. [Is it really long context if all you need is retrieval? towards genuinely difficult long context NLP](#). In *Proceedings of the 2024 Conference on Empirical Methods in Natural Language Processing*, pages 16576–16586, Miami, Florida, USA. Association for Computational Linguistics.
- Albert Gu and Tri Dao. 2024. [Mamba: Linear-time sequence modeling with selective state spaces](#). In *First Conference on Language Modeling*.
- Albert Gu, Karan Goel, and Christopher Re. 2022. [Efficiently modeling long sequences with structured state spaces](#). In *International Conference on Learning Representations*.
- Kaiming He, X. Zhang, Shaoqing Ren, and Jian Sun. 2015. [Delving deep into rectifiers: Surpassing human-level performance on imagenet classification](#). In *2015 IEEE International Conference on Computer Vision (ICCV)*, pages 1026–1034.
- Dan Hendrycks and Kevin Gimpel. 2016. [Gaussian error linear units \(gelus\)](#). *arXiv preprint arXiv:1606.08415*.
- Samy Jelassi, David Brandfonbrener, Sham M. Kakade, and Eran Malach. 2024. [Repeat after me: Transformers are better than state space models at copying](#). In *Proceedings of the 41st International Conference on Machine Learning*, volume 235 of *Proceedings of Machine Learning Research*, pages 21502–21521. PMLR.
- Tokio Kajitsuka and Issei Sato. 2024. [Are transformers with one layer self-attention using low-rank weight matrices universal approximators?](#) In *The Twelfth International Conference on Learning Representations*.
- Diederik P. Kingma and Jimmy Ba. 2015. [Adam: A method for stochastic optimization](#). In *The Third International Conference on Learning Representations*.
- Max Klabunde, Tobias Schumacher, Markus Strohmaier, and Florian Lemmerich. 2025a. [Similarity of neural network models: A survey of functional and representational measures](#). *ACM Computing Surveys*, 57(9):1–52.
- Max Klabunde, Tobias Schumacher, Markus Strohmaier, and Florian Lemmerich. 2025b. [Similarity of neural network models: A survey of functional and representational measures](#). *ACM Comput. Surv.*, 57(9).
- Simon Kornblith, Mohammad Norouzi, Honglak Lee, and Geoffrey Hinton. 2019. [Similarity of neural network representations revisited](#). In *Proceedings of the 36th International Conference on Machine Learning*, volume 97 of *Proceedings of Machine Learning Research*, pages 3519–3529. PMLR.
- Anne Lauscher, Vinit Ravishankar, Ivan Vulić, and Goran Glavaš. 2020. [From zero to hero: On the limitations of zero-shot language transfer with multilingual Transformers](#). In *Proceedings of the 2020 Conference on Empirical Methods in Natural Language Processing (EMNLP)*, pages 4483–4499, Online. Association for Computational Linguistics.
- Jiaheng Liu, Dawei Zhu, Zhiqi Bai, Yancheng He, Huanxuan Liao, Haoran Que, Zekun Wang, Chenchen Zhang, Ge Zhang, Jiebin Zhang, et al. 2025. [A comprehensive survey on long context language modeling](#). *arXiv preprint arXiv:2503.17407*.
- Nelson F. Liu, Kevin Lin, John Hewitt, Ashwin Paranjape, Michele Bevilacqua, Fabio Petroni, and Percy Liang. 2024. [Lost in the middle: How language models use long contexts](#). *Transactions of the Association for Computational Linguistics*, 12:157–173.
- Xin Men, Mingyu Xu, Qingyu Zhang, Qianhao Yuan, Bingning Wang, Hongyu Lin, Yaojie Lu, Xianpei Han, and Weipeng Chen. 2025. [Shortgpt: Layers in large language models are more redundant than you expect](#). In *Findings of the Association for Computational Linguistics: ACL 2025*, pages 20192–20204.
- Gonçalo Paulo, Thomas Marshall, and Nora Belrose. 2024. [Does transformer interpretability transfer to rnns?](#)
- Michael Poli, Stefano Massaroli, Eric Nguyen, Daniel Y Fu, Tri Dao, Stephen Baccus, Yoshua Bengio, Stefano Ermon, and Christopher Ré. 2023. [Hyena hierarchy: Towards larger convolutional language models](#). In *International Conference on Machine Learning*, pages 28043–28078. PMLR.
- Oscar Skean, Md Rifat Arefin, Yann LeCun, and Ravid Shwartz-Ziv. 2024. [Does representation matter? exploring intermediate layers in large language models](#). *arXiv preprint arXiv:2412.09563*.
- Oscar Skean, Md Rifat Arefin, Dan Zhao, Niket Nikul Patel, Jalal Naghiyev, Yann LeCun, and Ravid Shwartz-Ziv. 2025. [Layer by layer: Uncovering hidden representations in language models](#). In *Forty-second International Conference on Machine Learning*.
- Ian Smith, Janosch Ortmann, Farnoosh Abbas-Aghabazadeh, Petr Smirnov, and Benjamin Haibe-Kains. 2023. [On the distribution of cosine similarity with application to biology](#).

- Harald Steck, Chaitanya Ekanadham, and Nathan Kallus. 2024. [Is cosine-similarity of embeddings really about similarity?](#) In *Companion Proceedings of the ACM Web Conference 2024, WWW '24*, page 887–890, New York, NY, USA. Association for Computing Machinery.
- Ashish Vaswani, Noam Shazeer, Niki Parmar, Jakob Uszkoreit, Llion Jones, Aidan N Gomez, Łukasz Kaiser, and Illia Polosukhin. 2017. [Attention is all you need.](#) In *Advances in Neural Information Processing Systems*, volume 30. Curran Associates, Inc.
- Ivan Vulić, Edoardo Maria Ponti, Robert Litschko, Goran Glavaš, and Anna Korhonen. 2020. [Probing pretrained language models for lexical semantics.](#) In *Proceedings of the 2020 Conference on Empirical Methods in Natural Language Processing (EMNLP)*, pages 7222–7240, Online. Association for Computational Linguistics.
- Peihao Wang, Ruisi Cai, Yuehao Wang, Jiajun Zhu, Pragma Srivastava, Zhangyang Wang, and Pan Li. 2025. [Understanding and mitigating bottlenecks of state space models through the lens of recency and over-smoothing.](#) In *The Thirteenth International Conference on Learning Representations*.
- Thomas Wolf, Lysandre Debut, Victor Sanh, Julien Chaumond, Clement Delangue, Anthony Moi, Pierric Cistac, Tim Rault, Remi Louf, Morgan Funtowicz, Joe Davison, Sam Shleifer, Patrick von Platen, Clara Ma, Yacine Jernite, Julien Plu, Canwen Xu, Teven Le Scao, Sylvain Gugger, Mariama Drame, Quentin Lhoest, and Alexander Rush. 2020. [Transformers: State-of-the-art natural language processing.](#) In *Proceedings of the 2020 Conference on Empirical Methods in Natural Language Processing: System Demonstrations*, pages 38–45, Online. Association for Computational Linguistics.

A Mathematical Derivations

A.1 Mathematical Setups

The metric V_{glob}^2 measuring the variance of layer representations with $L = 1$ is defined as:

$$V_{\text{glob}}^2 \propto \|h^{(1)} - h^{(0)}\|^2 \quad (16)$$

where $h^{(l)}$ is the representation at layer l . Our goal is to compute the expected value $\mathbb{E}[V_{\text{glob}}^2]$. For both Transformers and Mamba, the representation evolves as:

$$h^{(1)} = h^{(0)} + F(h^{(0)}) \quad (17)$$

From our assumptions in §4.1, we have:

- $h^{(0)}, h^{(1)}$ are Gaussian matrices, $\mathbb{E}[h^{(0)}] = 0$ and $\text{Cov}(h^{(0)}) = \Sigma$. $h_t \sim N(0, \sigma^2 I)$.
- F is the update at layer 1 with deterministic parameters. We treat $F(x)$ as random matrices with $\mathbb{E}[F] = \mu_F$ and $\text{Cov}(F) = \Sigma_F$.
- $h_j^{(0)}$ and $h_t^{(0)}$ are independent for $j \neq t$ and $\mathbb{E}[h_j^{(0)}] = 0$ for all j , and $\mathbb{E}[h_i h_i^T] = \sigma^2 I_d$.
- $\mathbb{E}[h_j^{(0)} (h_t^{(0)})^T] = 0$ for $j \neq t$.

Objective: Under some mild assumptions, we simplify and compare St^2 from both architectures.

A.2 Proofs

Proof of Proposition 1. Substitute into Equation (16):

$$h^{(1)} - h^{(0)} = (h^{(0)} + F(h^{(0)})) - h^{(0)} = F(h^{(0)})$$

Thus:

$$V_{\text{glob}}^2 \propto \|h^{(1)} - h^{(0)}\|^2 = \|F(h^{(0)})\|^2$$

Denote $h^{(0)} \in \mathbb{R}^{n \times d}$, and $F : \mathbb{R}^{n \times d} \rightarrow \mathbb{R}^{n \times d}$, the squared Frobenius norm is:

$$\|F(h^{(0)})\|^2 = \sum_{i=1}^n \sum_{j=1}^d |F(h^{(0)})_{ij}|^2$$

The expectation is:

$$\mathbb{E}[\|F(h^{(0)})\|^2] = \mathbb{E} \left[\sum_{i,j} |F(h^{(0)})_{ij}|^2 \right] = \sum_{i,j} \mathbb{E}[|F(h^{(0)})_{ij}|^2]$$

Since F has deterministic parameters, the randomness in $F(h^{(0)})$ comes from $h^{(0)}$. The assumption states $\mathbb{E}[F(h^{(0)})] = \mu_F$, where $\mu_F \in \mathbb{R}^{n \times d}$, so:

$$\mathbb{E}[F(h^{(0)})_{ij}] = (\mu_F)_{ij}$$

The variance of $F(h^{(0)})$ is given by a covariance matrix Σ , but for a matrix-valued random variable, we interpret $\mathbb{E}[|F(h^{(0)})_{ij}|^2] = \text{Var}(F(h^{(0)})_{ij}) + |\mathbb{E}[F(h^{(0)})_{ij}]|^2$. Thus:

$$\mathbb{E}[|F(h^{(0)})_{ij}|^2] = \text{Var}(F(h^{(0)})_{ij}) + |(\mu_F)_{ij}|^2$$

Summing over all elements:

$$\mathbb{E}[\|F(h^{(0)})\|^2] = \sum_{i,j} \left(\text{Var}(F(h^{(0)})_{ij}) + |(\mu_F)_{ij}|^2 \right).$$

Thus, we have:

$$\mathbb{E}[V_{\text{glob}}^2] \propto \mathbb{E}[\|F(h^{(0)})\|^2] = \text{Tr}(\Sigma_F) + \|(\mu_F)\|^2 \quad (18)$$

□

From Equation (18), for Transformers:

$$\mathbb{E}[V_{\text{glob, Trans}}^2] \propto \text{Tr}(\Sigma_{F,\text{Trans}}) + \|\mu_{F,\text{Trans}}\|^2 \quad (19)$$

where:

- $F_{\text{Trans}} = \text{Attn}(h^{(0)}) + \text{FFN}(\tilde{h}^{(0)})$, $\tilde{h}^{(0)} = h^{(0)} + \text{Attn}(h^{(0)})$
- $\mu_{F,\text{Trans}} = \mathbb{E}[F_{\text{Trans}}] = \mathbb{E}[\text{Attn}(h^{(0)})] + \mathbb{E}[\text{FFN}(\tilde{h}^{(0)})]$
- $\Sigma_{F,\text{Trans}} = \text{Cov}(\text{Attn} + \text{FFN})$

For Mamba (a state-space model with selective mechanism):

$$\mathbb{E}[V_{\text{glob, Mamba}}^2] \propto \text{Tr}(\Sigma_{F,\text{Mamba}}) + \|\mu_{F,\text{Mamba}}\|^2 \quad (20)$$

where:

- $F_{\text{Mamba}} = \text{S6}(h') \circ z(h^{(0)})$, $z = \text{SiLU}(\text{Linear}(h^{(0)}))$, $h' = \text{SiLU}(\text{Conv1D}(\text{Linear}(h^{(0)})))$
- $\mu_{F,\text{Mamba}} = \mathbb{E}[\text{S6} \circ z] = \mathbb{E}[\text{S6}] \cdot \mathbb{E}[z] + \text{Cov}(\text{S6}, z)$
- $\Sigma_{F,\text{Mamba}} = \text{Cov}(\text{S6} \circ z)$

Proof of Proposition 2. Consider the effect of negating the input: if we replace x with $-x$:

$$Q_{\text{new}} = (-x)W_Q = -xW_Q = -Q, \quad K_{\text{new}} = (-x)W_K = -xW_K = -K, \quad V_{\text{new}} = (-x)W_V = -xW_V = -V$$

The new attention scores become:

$$\frac{(-Q)(-K)^T}{\sqrt{d_k}} = \frac{(-Q)(-K^T)}{\sqrt{d_k}} = \frac{QK^T}{\sqrt{d_k}}$$

Thus, the softmax remains unchanged:

$$\text{softmax} \left(\frac{(-Q)(-K)^T}{\sqrt{d_k}} \right) = \text{softmax} \left(\frac{QK^T}{\sqrt{d_k}} \right)$$

The output is:

$$\text{Attn}(-x) = \text{softmax} \left(\frac{Q_{\text{new}}K_{\text{new}}^T}{\sqrt{d_k}} \right) (V_{\text{new}}) = -\text{softmax} \left(\frac{QK^T}{\sqrt{d_k}} \right) V = -\text{Attn}(x)$$

This shows that the attention mechanism $\text{Attn}(x)$ is odd. □

Proof of Proposition 3. Because $\text{Attn}(h^{(0)})$ is odd and $h^{(l)}$ is symmetrically distributed, we have $\mathbb{E}[\text{Attn}(h^{(0)})] = \mathbb{E}[\text{Attn}(h^{(1)})] = 0$. □

Proof of Theorem 1. We have $\mu_{F, \text{Trans}} = \mathbb{E}[F_{\text{Trans}}] = \mathbb{E}[\text{Attn}(h^{(0)})] + \mathbb{E}[\text{FFN}(\tilde{h}^{(0)})]$ and $\mu_{h^{(0)}} = 0$. From Proposition 3, we have $\mathbb{E}[\text{Attn}(h^{(0)})] = 0$ and $\mathbb{E}[\tilde{h}^{(0)}] = \mathbb{E}[h^{(0)} + \text{Attn}(h^{(0)})] = 0$.

We have $\text{FFN}(\tilde{h}^{(0)}) = W_2(\text{GELU}(W_1\tilde{h}^{(0)} + b_1)) + b_2$ and assume that W_1, W_2, b_1, b_2 are independent, we approximate $\text{GELU}(a) \approx a \cdot \sigma(1.702a)$ following Hendrycks and Gimpel (2016), and further approximate $a \cdot \sigma(1.702a) \approx \frac{1}{2}a$ via Taylor expansion via removing higher-order terms, we have:

$$\mu_{F, \text{Trans}} = \mathbb{E}[\text{FFN}(\tilde{h}^{(0)})] = \mathbb{E}[W_2\text{GELU}(W_1\tilde{h}^{(0)} + b_1) + b_2] \quad (21)$$

$$\approx \mathbb{E}[W_2\frac{1}{2}(W_1\tilde{h}^{(0)} + b_1) + b_2] = \frac{1}{2}W_2b_1 + b_2 \quad (22)$$

□

Proof of Theorem 2. We need to compute $\text{Tr}(\Sigma_{F, \text{Trans}})$ for the Transformer-based model's update function $F_{\text{Trans}}(h^{(0)}) = \text{Attn}(h^{(0)}) + \text{FFN}(\tilde{h}^{(0)})$. We have:

$$F(h_t^{(0)}) = \text{Attn}(h_t^{(0)}) + \text{FFN}(\tilde{h}_t^{(0)}) \approx \text{Attn}(h_t^{(0)}) + \frac{1}{2}W_2(W_1\tilde{h}_t^{(0)} + b_1) + b_2 \quad (23)$$

$$= \text{Attn}(h_t^{(0)}) + \frac{1}{2}W_2W_1(h_t^{(0)} + \text{Attn}(h_t^{(0)})) + \frac{1}{2}W_2b_1 + b_2 \quad (24)$$

$$= \left(I + \frac{1}{2}W_2W_1\right) \text{Attn}(h_t^{(0)}) + \frac{1}{2}W_2W_1h_t^{(0)} + \frac{1}{2}W_2b_1 + b_2 \quad (25)$$

$$\therefore F_t = T_1\text{Attn}_t + T_2h_t + \mu \quad (26)$$

where $T_1 = I + \frac{1}{2}W_2W_1$, $T_2 = \frac{1}{2}W_2W_1$, and $\mu = \frac{1}{2}W_2b_1 + b_2$. We also denote F_t, Attn_t, h_t refers to $F(h_t^{(0)}), \text{Attn}(h_t^{(0)}), h_t^{(0)}$ respectively for ease of notation. We aim to compute $\Sigma_{F_t} = \mathbb{E}[F_tF_t^T] - \mathbb{E}[F_t]\mathbb{E}[F_t]^T$. Thus:

$$F_tF_t^T = (T_1\text{Attn}_t + T_2h_t + \mu)(T_1\text{Attn}_t + T_2h_t + \mu)^T \quad (27)$$

$$\therefore \mathbb{E}[F_tF_t^T] = T_1\mathbb{E}[\text{Attn}_t\text{Attn}_t^T]T_1^T + T_2\mathbb{E}[h_t h_t^T]T_2^T + \mu\mu^T \quad (28)$$

$$= T_1\Sigma_{\text{Attn}_t}T_1^T + T_2\Sigma_{h_t}T_2^T + \mu\mu^T \quad (29)$$

by using $\mathbb{E}[\text{Attn}_t] = \mathbb{E}[h_t] = 0$ and Attn_t depends on h_t , we have:

$$\Sigma_{F_t} = \mathbb{E}[F_tF_t^T] - \mathbb{E}[F_t]\mathbb{E}[F_t]^T \quad (30)$$

$$= T_1\Sigma_{\text{Attn}_t}T_1^T + T_2\Sigma_{h_t}T_2^T + T_1\text{Cov}(\text{Attn}_t, h_t)T_2^T + T_2\text{Cov}(\text{Attn}_t, h_t)^T T_1^T \quad (31)$$

Now we need to compute the covariance of the attention output, Σ_{Attn_t} . Given $h^{(0)} \in \mathbb{R}^{n \times d}$, the attention output for a single token t is:

$$\text{Attn}_t = \sum_{j=1}^n a_{tj}h_j^{(0)}W_V, \quad a_{tj} = \text{softmax}\left(\frac{(h_t^{(0)}W_Q)(h_j^{(0)}W_K)^T}{\sqrt{d_k}}\right) \quad (32)$$

As $\mathbb{E}[\text{Attn}_t] = 0$, the covariance matrix is:

$$\Sigma_{\text{Attn}_t} = \mathbb{E}[\text{Attn}_t\text{Attn}_t^T] = \mathbb{E}\left[\left(\sum_{j=1}^n a_{tj}h_j^{(0)}W_V\right)\left(\sum_{k=1}^n a_{tk}h_k^{(0)}W_V\right)^T\right] \quad (33)$$

$$= \mathbb{E}\left[\sum_{j,k=1}^n a_{tj}a_{tk}(h_j^{(0)}W_V)(h_k^{(0)}W_V)^T\right] \quad (34)$$

Since $h_j^{(0)}$ and $h_k^{(0)}$ are independent for $j \neq k$, and $\mathbb{E}[h_j^{(0)}] = \mathbb{E}[h_k^{(0)}] = 0$, the cross-terms vanish unless $j = k$:

$$\Sigma_{\text{Attn}_t} = \sum_{j=1}^n \mathbb{E}[a_{tj}^2] \mathbb{E}[(h_j^{(0)} W_V)(h_k^{(0)} W_V)^T] = \sum_{j=1}^n \mathbb{E}[a_{tj}^2] (W_V \Sigma_{h^{(0)}} W_V^T) \quad (35)$$

$$= \sum_{j=1}^n \mathbb{E}[a_{tj}^2] (\sigma^2 W_V W_V^T) = \sigma^2 \left(\sum_{j=1}^n \mathbb{E}[a_{tj}^2] \right) W_V W_V^T \quad (36)$$

The attention weights a_{tj} depend on the softmax output. For large d_k , the dot product $(h_t^{(0)} W_Q)(h_j^{(0)} W_K)^T / \sqrt{d_k}$ is approximately Gaussian. Assuming standard initialization ($W_Q, W_K \sim \mathcal{N}(0, 1/\sqrt{d})$), the variance of the dot product before scaling is:

$$\text{Var}((h_t^{(0)} W_Q)(h_j^{(0)} W_K)^T) \approx \sigma^2 \cdot \frac{1}{d} \cdot \sigma^2 \cdot d = \sigma^4 \quad (37)$$

$$\therefore \text{Var}\left(\frac{(h_t^{(0)} W_Q)(h_j^{(0)} W_K)^T}{\sqrt{d_k}}\right) \approx \frac{\sigma^4}{\sqrt{d_k}} \quad (38)$$

The softmax normalizes these scores, and for symmetrically distributed inputs, $\mathbb{E}[a_{tj}] \approx 1/n$. The variance of the softmax output is small, and we approximate $\mathbb{E}[a_{tj}^2] \approx 1/n^2$. And by assuming that $W_V W_V^T \approx I_d$ (standard initialization ensures $\text{Tr}(W_V W_V^T) \approx d$). The covariance Σ_{Attn_t} becomes:

$$\Sigma_{\text{Attn}_t} \approx \sigma^2 \left(\sum_{j=1}^n \frac{1}{n^2} \right) W_V W_V^T \approx \frac{\sigma^2}{n} I_d \quad (39)$$

Now we need to compute $\text{Cov}(\text{Attn}_t, h_t) = \mathbb{E}[\text{Attn}_t h_t] = \sum_{j=1}^t \mathbb{E}[a_{tj} v_j h_t^T]$. For $j \neq t$, v_j is independent of h_t and zero-mean so those terms are vanish. Thus, with $j = t$ and the same ‘‘mean-field’’ decoupling, we have:

$$\text{Cov}(\text{Attn}_t, h_t) \approx \mathbb{E}[a_{tt}] \mathbb{E}[v_t h_t^T] \quad (40)$$

$$= \frac{1}{n} W_V \mathbb{E}[h_t h_t^T] \quad (41)$$

$$= \frac{\sigma^2}{n} W_V \quad (42)$$

Put everything together, we have the covariance trace for token t as:

$$\text{Tr}(\Sigma_t) = \text{Tr}(T_1 \Sigma_{\text{Attn}_t} T_1^T) + \text{Tr}(T_2 \Sigma_{h_t} T_2^T) + 2\text{Tr}(T_1 \text{Cov}(\text{Attn}_t, h_t) T_2^T) \quad (43)$$

$$\approx \frac{\sigma^2}{n} \text{Tr}(T_1 T_1^T) + \sigma^2 \text{Tr}(T_2 T_2^T) + \frac{2\sigma^2}{n} \text{Tr}(T_1 W_V T_2^T) \quad (44)$$

Sum over t across n tokens, we finally have:

$$\text{Tr}(\Sigma_{F, \text{Trans}}) = \sigma^2 \text{Tr}(T_1 T_1^T) + n\sigma^2 \text{Tr}(T_2 T_2^T) + 2\sigma^2 \text{Tr}(T_1 W_V T_2^T) \quad (45)$$

□

Proof of Theorem 3. We have $\mu_{F, \text{Mamba}} = \mathbb{E}[\text{S6} \circ z]$. The S6 layer can be represented as a data-controlled linear operator (Poli et al., 2023; Ali et al., 2024). Specifically, for a sequence of inputs $h' = [h'_1, h'_2, \dots, h'_n]^T$, the outputs $o = [o_1, o_2, \dots, o_n]^T$ are computed through the following recursive equations. Assuming that $s_0 = 0$:

$$s_1 = \bar{B}_1 h'_1, \quad o_1 = C_1 \bar{B}_1 h'_1, \quad (46)$$

$$s_2 = \bar{A}_2 \bar{B}_1 h'_1 + \bar{B}_2 h'_2, \quad o_2 = C_2 \bar{A}_2 \bar{B}_1 h'_1 + C_2 \bar{B}_2 h'_2, \quad (47)$$

These equations define s_t and $h_t^{(1)}$ recursively using matrices \bar{A}_t , \bar{B}_t , and C_t , applied to input vectors h'_t . The general form, given in Equation (10), is:

$$s_t = \sum_{j=1}^t \left(\prod_{k=j+1}^t \bar{A}_k \right) \bar{B}_j h'_j, \quad o_t = C_t \sum_{j=1}^t \left(\prod_{k=j+1}^t \bar{A}_k \right) \bar{B}_j h'_j. \quad (48)$$

In matrix form, this can be expressed as:

$$o = \hat{\alpha} h', \quad (49)$$

where $\hat{\alpha}$ is the matrix:

$$\hat{\alpha} = \begin{bmatrix} C_1 \bar{B}_1 & 0 & 0 & \cdots & 0 \\ C_2 \bar{A}_2 \bar{B}_1 & C_2 \bar{B}_2 & 0 & \cdots & 0 \\ \vdots & \vdots & \ddots & \ddots & \vdots \\ C_n \bar{A}_n \bar{A}_{n-1} \cdots \bar{A}_2 \bar{B}_1 & C_n \bar{A}_n \bar{A}_{n-1} \cdots \bar{A}_3 \bar{B}_2 & \cdots & C_n \bar{B}_n & \end{bmatrix}. \quad (50)$$

The element at row i and column j of $\hat{\alpha}$, as specified in Equation (12), is computed as:

$$\hat{\alpha}_{i,j} = \begin{cases} C_i \left(\prod_{k=j+1}^i \bar{A}_k \right) \bar{B}_j & \text{if } i \geq j, \\ 0 & \text{if } i < j. \end{cases} \quad (51)$$

This matrix $\hat{\alpha} \in \mathbb{R}^{n \times n}$ is a function of the input and the parameters $\bar{A}, \bar{B}, \bar{C}, \bar{\Delta}$, encapsulating the data-controlled linear transformations applied by the S6 layer at layer l .

Next, we have $z = \text{SiLU}(\text{Linear}(h^{(0)}))$. Assume that $\text{Linear}(h^{(0)}) = W_z h^{(0)}$, where $W_z \in \mathbb{R}^{d \times ed}$ is a weight matrix and e is the expansion factor (typically 2). Denote $u = \text{Linear}(h^{(0)}) = W_z h^{(0)}$, by approximating SiLU function as $\text{SiLU}(x) \approx \frac{x}{2}$ via Taylor expansion, we have $z_i \approx \frac{u_i}{2}$. In other words, we have $\mathbb{E}[o_i z_i] \approx \mathbb{E}\left[o_i \frac{u_i}{2}\right] = \frac{1}{2} \mathbb{E}[o_i u_i]$. Computing $\mathbb{E}[o \circ z]$, we have:

$$\mathbb{E}[o \circ z] = \mathbb{E} \left[\begin{bmatrix} o_1 z_1 \\ \vdots \\ o_n z_n \end{bmatrix} \right] = \frac{1}{2} \mathbb{E} \left[\begin{bmatrix} o_1 u_1 \\ \vdots \\ o_n u_n \end{bmatrix} \right] = \frac{1}{2} \text{diag}(\mathbb{E}[o u^T]) \quad (52)$$

Substituting Equation (48), we have:

$$\mathbb{E}[o_t u_t^T] = \mathbb{E} \left[C_t \sum_{j=1}^t \left(\prod_{k=j+1}^t \bar{A}_k \right) \bar{B}_j h'_j (W_z h_t^{(0)})^T \right] \quad (53)$$

Now, for $h' = \text{SiLU}(\text{Conv1D}(\text{Linear}(h^{(0)})))$, assume that the linear transformation parameter is $W_h \in \mathbb{R}^{d \times ed}$ and the causal convolution with kernel size K (typically 4) is W_c , for the time $t \in \{1, 2, \dots, n\}$, we have:

$$h'_t = \text{SiLU}(\text{Conv1D}(\text{Linear}(h_t^{(0)}))) = \text{SiLU}(W_c(W_h h_t^{(0)})) \quad (54)$$

$$= \text{SiLU}\left(\sum_{j=0}^{K-1} W_{c_j}(W_h h_{t-j}^{(0)})\right) \approx \frac{1}{2} W_{c_j} W_h \sum_{j=0}^{K-1} h_{t-j}^{(0)} \quad (55)$$

Define $W_{h'_j} = W_{c_j} W_h$, where $W_{h'_j}$ is the combined transformation matrix. Thus:

$$\mathbb{E}[o_t u_t^T] = \mathbb{E}\left[C_t \sum_{i=1}^t \left(\prod_{k=i+1}^t \bar{A}_k\right) \bar{B}_i \left(\frac{1}{2} W_{h'_j} \sum_{j=0}^{K-1} h_{i-j}^{(0)}\right) (W_z h_t^{(0)})^T\right] \quad (56)$$

$$= \frac{1}{2} C_t \sum_{i=1}^t \sum_{j=0}^{K-1} \left(\prod_{k=i+1}^t \bar{A}_k\right) \bar{B}_i W_{h'_j} \mathbb{E}[h_{i-j}^{(0)} (h_t^{(0)})^T] W_z^T \quad (57)$$

Under assumptions, in the sum over $i = 1$ to t , the expectation $\mathbb{E}[h_{i-j}^{(0)} (h_t^{(0)})^T]$ is either 0 when $i - j \neq t$, or $\sigma^2 I_d$ when $i - j = t$, which means $i = t, j = 0$. Thus:

$$\mathbb{E}[o_t u_t^T] = \frac{1}{2} C_t \sum_{i=1}^t \sum_{j=0}^{K-1} \left(\prod_{k=i+1}^t \bar{A}_k\right) \bar{B}_i W_{h'_j} \mathbb{E}[h_{i-j}^{(0)} (h_t^{(0)})^T] W_z^T \quad (58)$$

$$= \frac{1}{2} C_t \left(\prod_{k=i+1}^t \bar{A}_k\right) \bar{B}_t W_{h'_0} \mathbb{E}[h_t^{(0)} (h_t^{(0)})^T] W_z^T \quad (59)$$

$$= \frac{1}{2} C_t \left(\prod_{k=i+1}^t \bar{A}_k\right) \bar{B}_t W_{h'_0} \sigma^2 W_z^T = \frac{\sigma^2}{2} C_t \bar{B}_t W_{h'_0} W_z^T \quad (60)$$

and $\mu_{F, \text{Mamba}} = \mathbb{E}[\text{S6} \circ z] = \frac{1}{2} \text{diag}(\mathbb{E}[ou^T]) = \frac{\sigma^2}{4n} \sum_{t=1}^n \text{diag}(C_t \bar{B}_t W_{h'_0} W_z^T)$. \square

Proof of Theorem 4. We need to compute $\text{Tr}(\Sigma_{F, \text{Mamba}}^2)$ for the Mamba model's update function $F_{\text{Mamba}}(h^{(0)}) = o \circ z$, where o is the output of the S6 layer and z is the gating term, both dependent on the input $h^{(0)}$.

Under the first-order nonlinearity approximation (S4), the Mamba update at time t is:

$$F(h_t^{(0)}) = \frac{1}{2} (o_t \circ z_t) \quad (61)$$

$$= \frac{1}{2} \text{diag}(W_z h_t^{(0)}) C_t \sum_{j=1}^t \left(\prod_{k=j+1}^t \bar{A}_k\right) \bar{B}_j W_{h'_j} h_j^{(0)} \quad (62)$$

$$= \frac{1}{2} \text{diag}(W_z h_t^{(0)}) \sum_{j=1}^t M_{t,j} h_j^{(0)}, \quad \text{where } M_{t,j} = C_t \left(\prod_{k=j+1}^t \bar{A}_k\right) \bar{B}_j W_{h'_j} \in \mathbb{R}^{ed \times d} \quad (63)$$

$$\mathbb{E}[F_t] = \frac{1}{2} \left(\sum_{j=1}^t \mathbb{E}[\text{diag}(W_z h_t^{(0)}) M_{t,j} h_j^{(0)}]\right) \quad (64)$$

where F_t refers to $F(h_t^{(0)})$ for ease of notation. For $j < t$, $h_j^{(0)}$ and $h_t^{(0)}$ are independent, so expectation is zero. For $j = t$, both terms involves $h_t^{(0)}$. Writing row r of $M_{t,t}$ as $m_{t,t,r}^T$ and row r of W_z as w_r^T :

$$\mathbb{E}[F_{t,r}] = \frac{1}{2} \mathbb{E}[(m_{t,t,r}^T h_t^{(0)})(w_r^T h_t^{(0)})] = \frac{\sigma^2}{2} m_{t,t,r}^T w_r \quad (65)$$

$$\therefore \mathbb{E}[F_t] = \frac{\sigma^2}{2} \text{diag}(M_{t,t} W_z^T) \quad (66)$$

For the second moment, use the identity $\text{diag}(a)X\text{diag}(b) = (ab^T) \circ X$, we can compute:

$$F_t F_t^T = \frac{1}{4} \text{diag}(W_z h_t^{(0)}) \left(\sum_{j=1}^t M_{t,j} h_j^{(0)} \right) \left(\sum_{m=1}^t M_{t,m} h_m^{(0)} \right)^T \text{diag}(W_z h_t^{(0)}) \quad (67)$$

$$= \frac{1}{4} \left[(W_z h_t^{(0)})(W_z h_t^{(0)})^T \right] \circ \left[\left(\sum_{j=1}^t M_{t,j} h_j^{(0)} \right) \left(\sum_{m=1}^t M_{t,m} h_m^{(0)} \right)^T \right] \quad (68)$$

Now take expectation: (1) for $j \neq m$, cross terms vanish by independence and zero mean; (2) for $j = m \neq t$, contributions are $\sigma^4 (W_z W_z^T) \circ (\sum_{j=1}^{t-1} M_{t,j} M_{t,j}^T)$; (3) for $j = m = t$, Isserlis's theorem gives an extra correction term. For $x \sim \mathcal{N}(0, \sigma^2 I)$ and vectors a, b, c, d ,

$$\mathbb{E}[(a^T x)(b^T x)(c^T x)(d^T x)] = \sigma^4 [(a \cdot b)(c \cdot d) + (a \cdot c)(b \cdot d) + (a \cdot d)(b \cdot c)]$$

With $a = m_{t,t,r}$, $b = w_r$, $c = m_{t,t,s}$, $d = w_s$, the (r, s) -entry of $\mathbb{E}[(W_z h_t)(W_z h_t)^T \circ (M_{t,t} h_t h_t^T M_{t,t}^T)]$ equals

$$\sigma^4 [(m_{t,t,r} \cdot w_r)(m_{t,t,s} \cdot w_s) + (m_{t,t,r} \cdot m_{t,t,s})(w_r \cdot w_s) + (m_{t,t,r} \cdot w_s)(w_r \cdot m_{t,t,s})]$$

In matrix form, the three terms correspond to

$$\sigma^4 [v v^T + (M_{t,t} M_{t,t}^T) \circ (W_z W_z^T) + (M_{t,t} W_z^T) \circ (W_z M_{t,t}^T)]$$

where $v = \text{diag}(M_{t,t} W_z^T)$. Putting everything together, we have:

$$\mathbb{E}[F_t F_t^T] = \frac{\sigma^4}{4} [v v^T + S_t \circ (W_z W_z^T) + (M_{t,t} W_z^T) \circ (W_z M_{t,t}^T)] \quad (69)$$

where $S_t = (\sum_{j=1}^{t-1} M_{t,j} M_{t,j}^T)$ and $v = \text{diag}(M_{t,t} W_z^T)$.

On the other hand, we have:

$$\mathbb{E}[F_t] \mathbb{E}[F_t]^T = \frac{\sigma^4}{4} \text{diag}(M_{t,t} W_z^T) [\text{diag}(M_{t,t} W_z^T)]^T = \frac{\sigma^4}{4} v v^T \quad (70)$$

Subtracting this, we have the covariance as:

$$\Sigma_{F_t} = \text{Cov}(F_t) = \mathbb{E}[F_t F_t^T] - \mathbb{E}[F_t] \mathbb{E}[F_t]^T \quad (71)$$

$$= \frac{\sigma^4}{4} [(W_z W_z^T) \circ S_t + (M_{t,t} W_z^T) \circ (W_z M_{t,t}^T)] \quad (72)$$

Take the trace and sum over t :

$$\text{Tr}(\Sigma_{F, \text{Mamba}}) = \frac{\sigma^4}{4} \{ \text{Tr}[(W_z W_z^T) \circ S_t] + \text{Tr}[(M_{t,t} W_z^T) \circ (W_z M_{t,t}^T)] \} \quad (73)$$

with $S_t = (\sum_{j=1}^{t-1} M_{t,j} M_{t,j}^T)$.

□

Proof of Theorem 5. Given that $\mathbb{E}[V_{\text{glob}}^2] = \|\mu_F\|^2 + \text{Tr}(\Sigma_F)$, we first rearrange all the equations we obtained.

(1) Transformer's mean. By Theorem 1,

$$\mu_{F,\text{Trans}} \approx \frac{1}{2}W_2b_1 + b_2.$$

Using independence and centering,

$$\mathbb{E}[\|\mu_{F,\text{Trans}}\|_2^2] = \frac{1}{4}\mathbb{E}[\|W_2b_1\|_2^2] + \mathbb{E}[\|b_2\|_2^2] = \alpha_T > 0$$

(2) Transformer's covariance. By Theorem 2,

$$\text{Tr}(\Sigma_{F,\text{Trans}}) = \sigma^2\text{Tr}(T_1T_1^T) + n\sigma^2\text{Tr}(T_2T_2^T) + 2\sigma^2\text{Tr}(T_1W_VT_2^T).$$

The cross term is linear in W_V and independent of W_1, W_2 . Since $\mathbb{E}[W_V] = 0$, we have:

$$\mathbb{E}[\text{Tr}(\Sigma_{F,\text{Trans}})] = \sigma^2\mathbb{E}[\text{Tr}(T_1T_1^T)] + n\sigma^2\mathbb{E}[\text{Tr}(T_2T_2^T)].$$

Now computing:

$$\begin{aligned} \text{Tr}(T_1T_1^T) &= \text{Tr}\left[\left(I + \frac{1}{2}W_2W_1\right)\left(I + \frac{1}{2}W_2W_1\right)^T\right] \\ &= \text{Tr}\left[I + \frac{1}{2}W_2W_1 + \frac{1}{2}(W_2W_1)^T + \frac{1}{4}(W_2W_1)(W_2W_1)^T\right] \\ &= d + \text{Tr}(W_2W_1) + \frac{1}{4}\|W_2W_1\|_F^2 \\ \text{Tr}(T_2T_2^T) &= \frac{1}{4}\|W_2W_1\|_F^2 \end{aligned}$$

Putting together, we get:

$$\begin{aligned} \mathbb{E}[\text{Tr}(\Sigma_{F,\text{Trans}})] &= \sigma^2\mathbb{E}[\text{Tr}(T_1T_1^T)] + n\sigma^2\mathbb{E}[\text{Tr}(T_2T_2^T)] \\ &= \sigma^2\mathbb{E}\left[d + \text{Tr}(W_2W_1) + \frac{(n+1)}{4}\|W_2W_1\|_F^2\right] \\ &= \frac{\sigma^2n}{4}\mathbb{E}[\|W_2W_1\|_F^2] + \sigma^2\left[\mathbb{E}[\text{Tr}(W_2W_1)] + \frac{1}{4}\mathbb{E}[\|W_2W_1\|_F^2] + d\right] \\ &= \frac{\sigma^2n}{4}\beta_T + \sigma^2\gamma_T \end{aligned}$$

where $\beta_T > 0$ and $\gamma_T \geq d > 0$ are constants, given that W_1, W_2 are independent and centered.

(3) Mamba's mean. By Theorem 3,

$$\mu_{F,\text{Mamba}} \approx \frac{\sigma^2}{4n} \sum_t \text{diag}(C_t \bar{B}_t W_h^0 W_z^T).$$

Using Jensen and $\|\text{diag}(X)\|_2 \leq \|X\|_F$,

$$\|\mu_{F,\text{Mamba}}\|_2^2 \leq \frac{\sigma^4}{16n^2} \sum_t \|C_t \bar{B}_t W_h^0 W_z^T\|_F^2 \leq \frac{\sigma^4}{16n^2} \alpha_M.$$

where $\alpha_M > 0$ is a constant.

(4) Mamba's covariance. By Theorem 4, with $M_{t,j} = C_t(\prod_{k=j+1}^t \bar{A}_k) \bar{B}_j W_{h'}$ and $S_t = \sum_{j<t} M_{t,j} M_{t,j}^T$,

$$\text{Tr}(\Sigma_{F,\text{Mamba}}) = \frac{\sigma^4}{4} \left\{ \text{Tr}[(W_z W_z^T) \circ S_t] + \text{Tr}[(M_{t,t} W_z^T) \circ (W_z M_{t,t}^T)] \right\}.$$

Assume that Mamba model is uniformly contractive: there exists $\rho \in (0, 1)$ with $\|\bar{A}_t\|_2 \leq \rho$ for all t , and bounded operator/Frobenius norms $\|C_t\|_2 \leq c$, $\|\bar{B}_t\|_2 \leq b$, $\|W_{h'}\|_2 \leq h$, $\|W_z\|_F \leq z$.

Using $\text{Tr}(XY) \leq \|X\|_F \|Y\|_F$ and contractivity bounds,

$$\sum_{j<t} \|M_{t,j}\|_F^2 \leq \frac{c^2 b^2 h^2}{1 - \rho^2}, \quad \|M_{t,t}\|_F^2 \leq c^2 b^2 h^2.$$

Therefore,

$$\text{Tr}(\Sigma_{F,\text{Mamba}}) \leq \frac{\sigma^4}{4} z^2 c^2 b^2 h^2 \left(1 + \frac{1}{1 - \rho^2}\right) = \frac{\sigma^4}{4} \beta_M.$$

where $\beta_M > 0$ is a constant.

(5) Comparison and Threshold. Collecting the bounds above, we have:

$$\begin{aligned} \mathbb{E}[V_{\text{glob, Trans}}^2] &= \mathbb{E}\|\mu_{F,\text{Trans}}\|_2^2 + \mathbb{E}[\text{Tr}(\Sigma_{F,\text{Trans}})] = \frac{\sigma^2 n}{4} \beta_T + \sigma^2 \gamma_T + \alpha_T \\ \mathbb{E}[V_{\text{glob, Mamba}}^2] &= \mathbb{E}\|\mu_{F,\text{Mamba}}\|_2^2 + \mathbb{E}[\text{Tr}(\Sigma_{F,\text{Mamba}})] \leq \frac{\sigma^4}{16n^2} \alpha_M + \frac{\sigma^4}{4} \beta_M \end{aligned}$$

Cubic form. Define the cubic polynomial

$$Q(n) = an^3 + bn^2 + d,$$

with

$$a := 4\sigma^2 \beta_T, \quad b := 16\sigma^2 \gamma_T + 16\alpha_T - 4\sigma^4 \beta_M, \quad d := -\sigma^4 \alpha_M.$$

Special case $n = 1$: We aim to prove that $Q(1) > 0$ in practice:

$$\begin{aligned} Q(1) &= 4\sigma^2 \beta_T + 16\sigma^2 \gamma_T + 16\alpha_T - 4\sigma^4 \beta_M - \sigma^4 \alpha_M \\ &= 16\alpha_T + 4\sigma^2 (\beta_T + 4\gamma_T) - \sigma^4 (4\beta_M + \alpha_M) \end{aligned}$$

Let $x = \sigma^2$, then

$$\begin{aligned} Q(1) &= -(4\beta_M + \alpha_M)x^2 + 4(\beta_T + 4\gamma_T)x + 16\alpha_T > 0 \\ \therefore & \quad (4\beta_M + \alpha_M)x^2 - 4(\beta_T + 4\gamma_T)x - 16\alpha_T < 0 \end{aligned}$$

Solve quadratic equality for x , we have:

$$\begin{aligned} x &= \frac{4(\beta_T + 4\gamma_T) \pm \sqrt{16(\beta_T + 4\gamma_T)^2 + 64(4\beta_M + \alpha_M)\alpha_T}}{2(4\beta_M + \alpha_M)} \\ &= \frac{4(\beta_T + 4\gamma_T) \pm 4\sqrt{(\beta_T + 4\gamma_T)^2 + 4(4\beta_M + \alpha_M)\alpha_T}}{2(4\beta_M + \alpha_M)} \\ &= \frac{(\beta_T + 4\gamma_T) + \sqrt{(\beta_T + 4\gamma_T)^2 + 4(4\beta_M + \alpha_M)\alpha_T}}{2\beta_M + \alpha_M/2} \end{aligned}$$

Note that we take the positive root with “+” because the parabola opens downward (coefficient of x^2 negative in original $Q(1)$) and the solution with “+” gives the upper bound.

Hence, $Q(1) > 0$ if and only if:

$$\sigma^2 \leq x_{\max} := \frac{(\beta_T + 4\gamma_T) + \sqrt{(\beta_T + 4\gamma_T)^2 + 4(4\beta_M + \alpha_M)\alpha_T}}{2\beta_M + \alpha_M/2}$$

Given that $\alpha_T > 0, \beta_T > 0, \alpha_M > 0, \beta_M > 0$, we have:

$$\frac{(\beta_T + 4\gamma_T) + \sqrt{(\beta_T + 4\gamma_T)^2 + 4(4\beta_M + \alpha_M)\alpha_T}}{4\beta_M + \alpha_M} \geq \frac{4\gamma_T + \sqrt{(4\gamma_T)^2 + 0}}{4\beta_M + \alpha_M} = \frac{8\gamma_T}{4\beta_M + \alpha_M}.$$

Since $\gamma_T \geq d > 0$ and $\beta_M, \alpha_M > 0$ are small, this implies

$$\sigma_{\max}^2 \gg 1.$$

Hence, for any typical choice of $\sigma^2 \in (0, 1)$, we have

$$\sigma^2 < 1 \ll \sigma_{\max}^2 \implies Q(1) > 0.$$

General case $n \geq 1$: As $Q(1) = a + b + d > 0, d < 0$, then $a + b > 0$. We now compare $Q(n)$ vs $Q(1)$.

$$\begin{aligned} Q(n) - Q(1) &= an^3 + bn^2 - a - b \\ &= a(n-1)(n^2 + n + 1) + b(n-1)(n+1) \\ &= (n-1)[an^2 + (a+b)(n+1)] > 0 \quad \forall n > 1 \\ \therefore Q(n) &> Q(1) > 0 \quad \forall n > 1 \end{aligned}$$

Therefore, we conclude that $Q(n) > 0 \quad \forall n \geq 1 \Leftrightarrow \mathbb{E}[V_{\text{glob, Trans}}^2] > \mathbb{E}[V_{\text{glob, Mamba}}^2] \quad \forall n \geq 1.$ □

A.3 Multi-layer Variance: From $L=1$ to L -layer model

Setup and notation. Let $h^{(0)}, h^{(1)}, \dots, h^{(L)} \in \mathbb{R}^{n \times d}$ be the layer activations with $h^{(l+1)} = F_l(h^{(l)})$ for blocks F_l (Transformer or Mamba), and write layer increments $\Delta^{(l)} \triangleq h^{(l+1)} - h^{(l)}$ and the layerwise mean $\bar{h} \triangleq \frac{1}{L+1} \sum_{l=0}^L h^{(l)}$. Define the path energy $\mathcal{E}_{\text{path}} \triangleq \sum_{l=0}^{L-1} \|\Delta^{(l)}\|_F^2$ and the L -layer variance

$$V_{\text{glob}}^2 \triangleq \frac{1}{nd} \cdot \frac{1}{L+1} \sum_{l=0}^L \|h^{(l)} - \bar{h}\|_F^2.$$

Assumption 5 (Layer-wise centering and sub-Gaussianity). *Each layer input is centered and standardized by normalization (e.g., LayerNorm), so rows of $h^{(l)}$ are zero-mean, isotropic, sub-Gaussian with bounded second/fourth moments; learned affine shifts are tracked in means and do not affect covariances after centering.*

Assumption 6 (Weak dependence across tokens). *Token rows form a weakly dependent process (e.g., α -mixing or Ψ -weak dependence) with summable coefficients, so cross-token covariance terms are bounded by mixing coefficients times Lipschitz moduli of F_l .*

Assumption 7 (Block Lipschitz/contractivity). *Each block F_l is (piecewise) Lipschitz with $\text{Lip}(F_l) \leq \Lambda_l$, and Mamba satisfies uniform contractivity for state updates with $\|\bar{A}_t\| \leq \rho < 1$ and bounded operators $\|C_t\| \leq c, \|\bar{B}_t\| \leq b, \|W_{h'}\| \leq h, \|W_z\|_F \leq z$, as in your one-layer bounds.*

Lemma 1 (Discrete Poincaré on a chain). *For the sequence $\{h^{(l)}\}_{l=0}^L$ it holds that*

$$\sum_{l=0}^L \|h^{(l)} - \bar{h}\|_F^2 \leq \frac{1}{4 \sin^2\left(\frac{\pi}{2(L+1)}\right)} \sum_{l=0}^{L-1} \|h^{(l+1)} - h^{(l)}\|_F^2,$$

and thus $V_{\text{glob}}^2 \leq \frac{1}{4nd \sin^2\left(\frac{\pi}{2(L+1)}\right)} \mathcal{E}_{\text{path}}$.

Lemma 2 (Propagation of one-layer surrogates). Write $\Delta^{(l)} = F_l(h^{(l)}) - h^{(l)}$. Then for any $0 \leq l \leq L-1$,

$$\|h^{(l+1)} - h^{(l)}\|_F \leq \left(\prod_{k=l+1}^L \Lambda_k \right) \|F_l(h^{(l)})\|_F,$$

and in SSM blocks the product admits $\prod_{k=l+1}^L \Lambda_k \leq C \rho^{L-l}$ by uniform contractivity.

Remark. The Lipschitz constants $\{\Lambda_l\}$ control how single-layer surrogates propagate to later layers. If $\prod_{k=l+1}^L \Lambda_k$ remains bounded by a modest constant, the per-layer bounds in Lemma 2 give tight control on path increments. For SSMs, uniform contractivity $\|\bar{A}_t\| \leq \rho < 1$ yields the geometric bound $\prod_{k=l+1}^L \Lambda_k \leq C \rho^{L-l}$ used below.

Proof. By Lipschitz continuity of the blocks, for any $r > l$,

$$\|h^{(r)} - h^{(r-1)}\|_F = \|F_{r-1}(h^{(r-1)}) - F_{r-1}(h^{(r-2)})\|_F \leq \Lambda_{r-1} \|h^{(r-1)} - h^{(r-2)}\|_F,$$

and iterating this bound from $r = l + 1$ up to $r = L$ gives

$$\|h^{(l+1)} - h^{(l)}\|_F \leq \left(\prod_{k=l+1}^L \Lambda_k \right) \|F_l(h^{(l)})\|_F.$$

The SSM contractivity statement follows by replacing Λ_k with ρ for SSM blocks. \square

Assumption 8 (Uniform one-layer gap - quantitative form). There exists $\delta > 0$ such that under matched capacity/initialization and Assumptions 5–7,

$$\mathbb{E} \left[\|F_l(h^{(l)})\|_F^2 \right]_{\text{Trans}} \geq (1 + \delta) \mathbb{E} \left[\|F_l(h^{(l)})\|_F^2 \right]_{\text{Mamba}} \quad \text{for all } l \in \{0, \dots, L-1\}.$$

Theorem 6 (L -layer variance ordering). Under Assumptions 5–8, the expected path energies obey

$$\mathbb{E}[\mathcal{E}_{\text{path}}]_{\text{Trans}} \geq \mathbb{E}[\mathcal{E}_{\text{path}}]_{\text{Mamba}},$$

and the L -layer stabilities satisfy

$$\mathbb{E}[V_{\text{glob}}^2]_{\text{Trans}} \geq \mathbb{E}[V_{\text{glob}}^2]_{\text{Mamba}}.$$

Proof. From Lemma 2 we have $\|\Delta^{(l)}\|_F^2 \leq \kappa_l^2 \|F_l(h^{(l)})\|_F^2$ where $\kappa_l := \prod_{k=l+1}^L \Lambda_k$. Taking expectations and summing over l yields

$$\mathbb{E}[\mathcal{E}_{\text{path}}] \leq \sum_{l=0}^{L-1} \kappa_l^2 \mathbb{E}[\|F_l(h^{(l)})\|_F^2].$$

By Assumption 8 (quantitative form) each term for the Transformer dominates the Mamba counterpart by factor $(1 + \delta)$, hence $\mathbb{E}[\mathcal{E}_{\text{path}}]_{\text{Trans}} \geq \mathbb{E}[\mathcal{E}_{\text{path}}]_{\text{Mamba}}$, up to the (uniformly controlled) factors $\{\kappa_l\}$. Finally apply Lemma 1 and normalize by $nd(L+1)$ to obtain the stated ordering for St_L^2 . \square

Corollary A.1 (Transformer vs. Mamba). If each Transformer block's one-layer bound dominates the Mamba counterpart as established in your $L=1$ analysis, then the L -layer ordering $\mathbb{E}[V_{\text{glob}}^2]_{\text{Trans}} \geq \mathbb{E}[V_{\text{glob}}^2]_{\text{Mamba}}$ holds for all $L \geq 1$, with constants depending on $\{\Lambda_l\}$ and SSM contractivity ρ .

Remarks. (i) The discrete Poincaré constant $(L+1)^2/\pi^2$ is tight for a chain and can be replaced with any equivalent spectral constant of the path graph; constants do not affect the ordering conclusion, only prefactors; (ii) Assumptions 5–6 replace per-layer Gaussianity/independence with practical layer-wise centering and weak dependence; (iii) Learned affine shifts from normalization affect means but not covariances after centering, and can be tracked separately in μ_F terms as in your $L=1$ derivations.

B Prompting Details

Following setup by Liu et al. (2024) and Gao et al. (2024), we construct key-value pairs retrieval and multi-document question answering prompting dataset. Representative samples from each appear below, sourced from Gao et al. (2024).

Key-Value pairs retrieval (kv-pairs) We generate n pairs of 128-bit randomly generated UUID.

Example Key-Value pair

```
"7f666c61-573f-4212-a0a9-6f90d487cd4a" : "2a1d0ba0-cfe4-4df5-987a-6ee1be2c6ac0"
```

The n kv-pairs are composed into one single JSON object. To test at ID k , we choose one pair as gold, insert it at ID k , and then construct as a prompt in the format:

Extract the value corresponding to the specified key in the JSON object below.

JSON data:

```
{ "key1": "value1",  
  "key2": "value2",  
  ...  
  "keyk": "valuek",  
  ...  
  "keyn": "valuen",  
}
```

Key: "key^k"

Corresponding value:

Multi-document question answering (MDQA) In the n document setting, we randomly select one question answer pair from the dataset by Liu et al. (2024). Subsequently we retrieve the document containing this answer and mark it as gold.

Example retrieval

Question: who got the first nobel prize in physics

Answer: Wilhelm Conrad Röntgen

Document: (Title: List of Nobel laureates in Physics) The first Nobel Prize in Physics was awarded in 1901 to Wilhelm Conrad Röntgen, of Germany, who received...

We then sample $n - 1$ distractors, relevant documents that do not contain the answer. To test at ID k , we randomly shuffle the distractors and then insert the gold document at ID k . Example prompt with gold document at ID k is like:

Write a high-quality answer for the given question using only the provided search results (some of which might be irrelevant).

Document [1](Title: Asian Americans in science and technology) Prize in physics for discovery of the subatomic...

...

Document [k](Title: List of Nobel laureates in Physics) The first Nobel Prize in Physics was awarded in 1901...

...

Document [n] (Title: Scientist) and pursued through a unique method, was essentially in place. Ramón y Cajal won ...

Question: who got the first nobel prize in physics

Answer:

C Ablation Study on Random Initialization

To rigorously test whether the early oversmoothing observed in TBMs at random initialization is an intrinsic architectural property rather than a residual-copy artifact or normalization effect, we conducted a systematic ablation study measuring inter-token cosine similarity under controlled modifications to the model forward pass.

C.1 Experimental Setup

We expand the experiments in §3.2 with three key ablations:

- **Residual bias control:** Compute InterSim on $\Delta h^{(l)} = h^{(l+1)} - h^{(l)}$ to isolate non-residual update effects (Fig. 5).
- **Normalization ablation:** Baseline LN, fully disabled LN, and LN affine reset ($\gamma = 1, \beta = 0$) (Fig. 6).
- **Embedding scaling:** Scale embedding outputs by $\{0.5, 1.0, 2.0\}$ (Fig. 7).

C.2 Results

Residual bias control (Fig. 5) : TBMs remain systematically more oversmoothed than SSMs when measuring InterSim on residual *updates* Δh rather than full hidden states. The gap persists (though absolute InterSim decreases due to loss of skip-copy), confirming TBM blocks produce more homogenizing updates even after removing the trivial identity path.

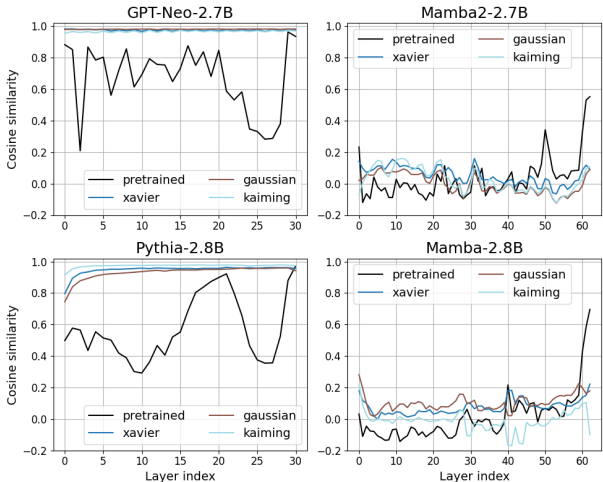


Figure 5: Layer-wise probing accuracy of TBMs (left) and SSMs (right) with $n = 2K$ tokens. Delta computed as $\Delta = h^{(l+1)} - h^{(l)}$ to isolate non-residual effects.

Normalization ablation (Fig. 6) : Disabling LayerNorm causes a dramatic collapse in TBM InterSim, while resetting affine parameters ($\gamma = 1, \beta = 0$) produces intermediate behavior. This reveals normalization as a key mechanistic contributor to TBM’s early token homogenization at initialization.

Embedding scaling (Fig. 7) : The TBM > SSM oversmoothing ordering remains qualitatively stable across a 4x range of embedding scales $\{0.5, 1.0, 2.0\}$, ruling out activation magnitude as the primary driver of the observed gap.

C.3 Discussion

These results localize TBM oversmoothing at random initialization to the *joint interaction* of residual pathways, LayerNorm preconditioning, and global self-attention mixing. The persistence of TBM > SSM gaps under Δh analysis and embedding scaling provides strong evidence against trivial “skip-copy bias” or “norm-rescaling artifact” explanations.

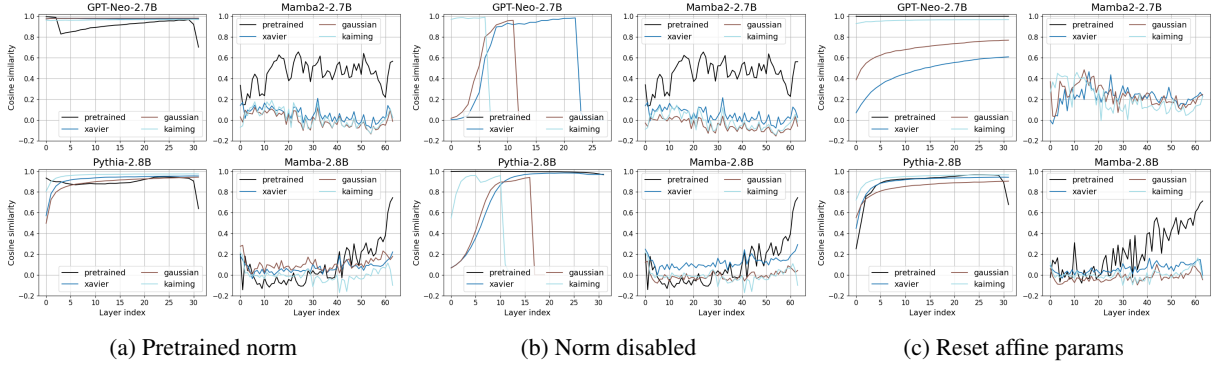


Figure 6: Effect of embedding layer normalization variants under random initializations.

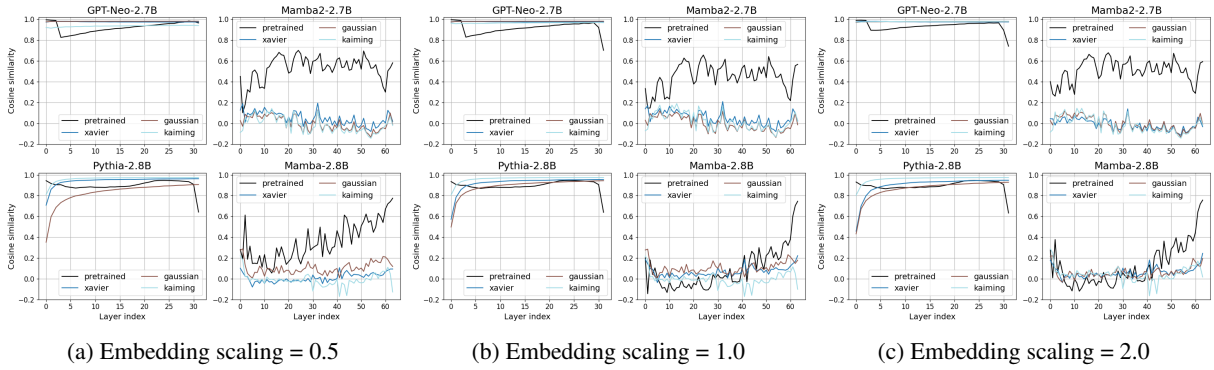


Figure 7: Effect of embedding scaling on random initialization.

While LayerNorm ablation reveals its mechanistic importance, this is expected—modern TBMs are specifically architected around pre-/post-LN residual blocks. The oversmoothing bias emerges from this full design rather than attention in isolation. In contrast, SSM mixer blocks (selective scan + gating) produce substantially less homogenization across all conditions, requiring training to develop comparable token collapse.

This architectural distinction—global mixing with normalization vs. local recurrent refinement—underpins the divergent representation dynamics observed throughout the paper.